Decoding Air-Exposure Degradation Chemistry and Improving Strategy for

Layered Sodium Transition Metal Oxide Cathodes

Feng Li¹, Wei Tang¹, Junlin Wu², Lanshuang Zhang², Anthony Mu¹, and Zheng Chen^{1, 2, 3} * ¹Aiiso Yufeng Li Family Department of Chemical and Nano Engineering, University of California, San Diego, La Jolla, California 92093, United States ²Program of Materials Science Engineering, University of California, San Diego, La Jolla, California 92093, **United States** ³Sustainable Power and Energy Center, University of California, San Diego, La Jolla, California 92093, United States *Correspondence to: <u>zhc199@ucsd.edu</u> (Z.C.)

Abstract

Developing suitable cathodes of sodium-ion batteries (SIBs) with robust electrochemical performance and industrial application potential is crucial for the commercialization of large-scale stationary energy storage systems. Layered sodium transition metal oxides, Na_xTmO₂ (Tm representing transition metal), possessing considerable specific capacity, high operational potential, facile synthesis, cost-effectiveness, and environmentally friendly characteristics, stand out as viable cathode materials. Nevertheless, the prevailing challenge of air-induced degradation in most Na_xTmO₂ significantly increases costs associated with production, storage, and transportation, coupled with a rapid decay in reversible capacity. This inherent obstacle inevitably impedes the advancement and commercial viability of SIBs. To address this challenge, it is essential to decode the chemistry of degradation caused by air exposure and develop protective strategies accordingly. In this review, we provide a comprehensive and in-depth understanding of the fundamental mechanisms associated with air-induced degradation. Additionally, we explore the current state-of-the-art effective protective strategies and discuss the corresponding sustainability and scalability features. This review concludes with an outlook on present and future research directions concerning air-stable cathode materials, offering potential avenues for upcoming investigations in advancing alkali metal layered oxides.

1. Introduction

Effectively storing and utilizing clean and renewable energy is pivotal for realizing carbon neutrality by the mid-21st century and mitigating the severe effects of global climate change^[1]. In response to this imperative, sodium-ion batteries (SIBs) stand out as the most promising solution for large-scale stationary energy storage^[2]. Several factors are paramount in the process of promoting the commercialization and application of SIBs. One critical factor is calendar lifetime, which pertains to the long-term durability of the batteries. Another important aspect is capacity and safety, crucial for ensuring both efficiency and reliability of the batteries in practical application. Additionally, the manufacturing and operational costs play an important role as they influence the economic feasibility of SIBs^[3]. These factors are directly linked to the components that constitute the SIBs. Evidently, SIBs naturally capitalize on the abundant and geographically homogeneous sodium resources^[2a, 4], low-cost lighter aluminum current collectors in conjunction with environmentally friendly hard carbon anodes^[5], ensuring both sustainable supply chain and economic viability^[6]. Currently, a crucial factor in achieving the industrial production of SIBs is the development of suitable cathodes^[7], which not only significantly influences the overall energy density but also serves as the key determinant in the production costs of SIBs, accounting for as much as 26% of the total cell costs (**Figure 1a**).

In recent decades, tremendous efforts have been made to explore promising cathodes for SIBs by focusing on cost-effective precursors (**Figure 1b**). Representative desired cathodes are illustrated in **Figure 1c-e**, including layered transition metal oxides (Na_xTmO₂, Tm represents transition metal)^[7-8], Prussian blue analogues (Na_xTm₁Tm₂(CN)₆, Tm₁ and Tm₂ represent different transition metals)^[9], and polyanionic compounds (Na_xTm_y(XO₄)_n, Tm represents transition metal, X represents S, P, Si, As, Mo, and W)^[10]. In recent years, research institutes and pioneering companies all over the world have made significant strides toward the exploration and early commercialization of SIBs, emphasizing strong performance and enhanced safety features. Na_xTmO₂ (0.5 \leq x \leq 1) has become the most rapidly industrialized cathode of SIBs, owing to its comprehensive performance (**Figure 1f**)^[8c, 11]. When viewed from a materials standpoint, it stands out with higher energy density, lifespan and cost-effectiveness compared to other cathode options, making it a prime candidate for practical applications.

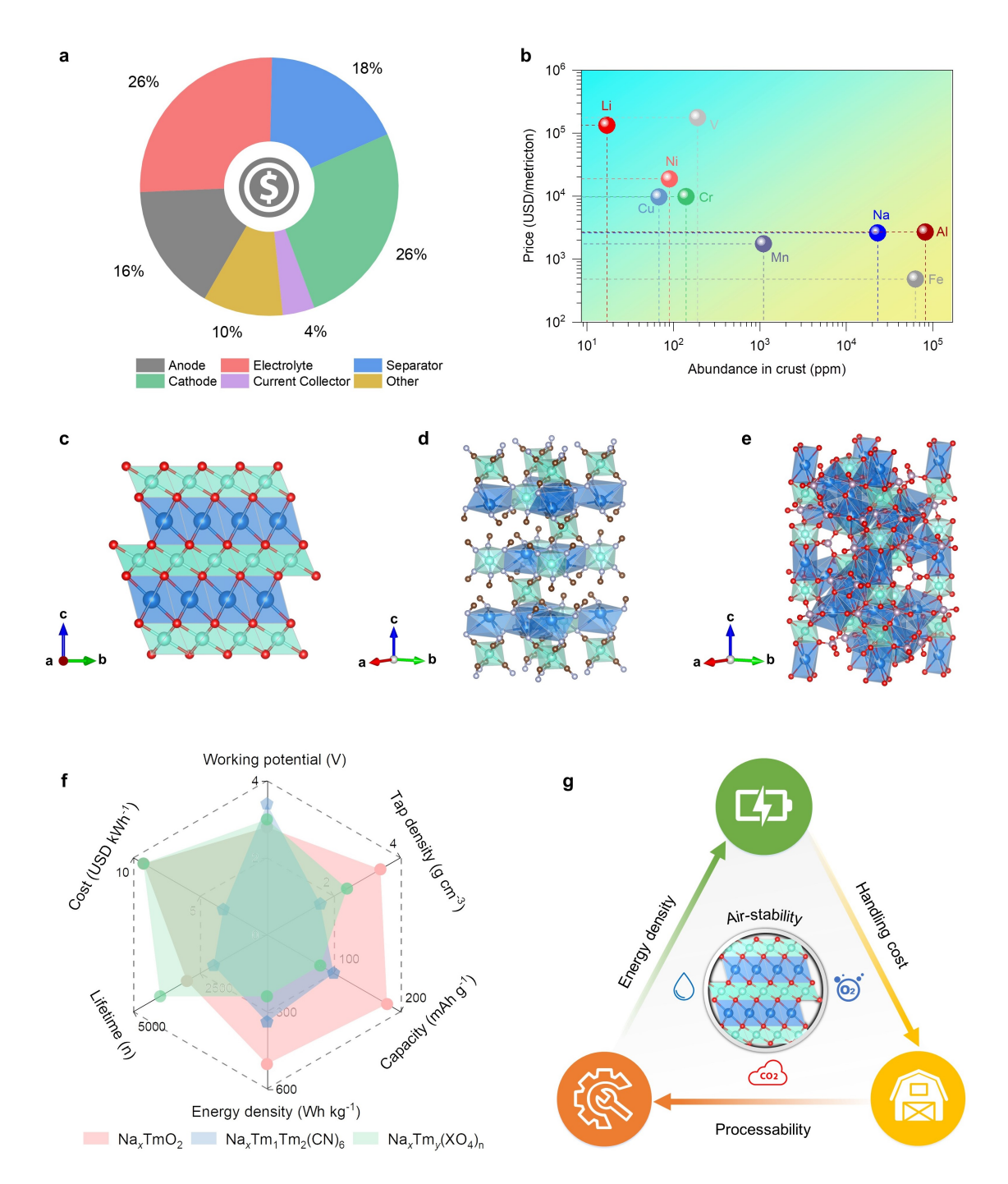


Figure 1. (a) Analysis of cost proportion of SIBs, including anode, electrolyte, separator, cathode, current collector, and other components^[12]; (b) Abundance in crust^[13] and unit price^[14] analysis of primary precursor; (c-e) Crystal structure of layered transition metal oxides, Prussian blue analogues, and polyanionic compounds, crystal structure visualization enabled by VESTA; (f) Radar map for working potential, tap density, capacity, energy density, lifetime, and cost analysis of cathodes; (g) Key factors to be considered for commercialization of SIBs^[3a, 15].

In the field of Na_xTmO_2 , there is a clear emphasis on impressive electrochemical performances, whereas the importance of storage characteristics tends to be overlooked. However, as with electrochemical performance, the processability and handling cost (**Figure 1g**), which are determined

by storage characteristics, are equally important and nonnegligible factors for the practical application of SIBs, especially considering their targeted applications in large-scale grid energy storage^[2a, 16]. The air stability of cathode processing affects the entire lifecycle of SIBs, from production to storage, battery fabrication and application, involving additional costs in terms of facilities, packaging, operational and service procedures^[2e, 3a, 17]. Unfortunately, the majority of Na_xTmO₂ cathodes have a fatal issue: hygroscopic characteristics, even with a period of exposure to the ambient atmosphere[11c, ^{18]}. This results in substantial loss of capacity and significantly increased handling costs, posing a hindrance to the further development of competitive SIBs.

Therefore, it is crucial to understand the degradation mechanism caused by air exposure, figure out corresponding chemistries, and subsequently improve the storage characteristics of Na_xTmO₂ to ensure their practical applicability^[19]. In this review, we are committed to providing a comprehensive and cutting-edge understanding of the air degradation chemistries of Na_xTmO₂. We begin by sorting out and analyzing the fundamental structure and intrinsic origins of the instability of Na_xTmO₂, offering a detailed mechanism of degradation induced by H₂O, CO₂, and O₂. Subsequently, we carefully consider the impact of air-induced degradation of Na_xTmO₂ on various aspects of the production process of SIBs, ranging from the material manufacturing to the battery assembly level. Finally, we provide discussions of solutions to improve air-stability of Na_xTmO₂ based on recent developments, aiming to minimize the gap between theoretical understanding and practical application. This review could provide valuable insights for the research community to address air-sensitivity issues in handling processes and develop air-durable Na_xTmO₂.

2. Air-degradation mechanisms of layered Na_xTmO₂

Layered Na_xTmO₂ consists of co-edge connected [TmO₆] octahedra (where Tm represents a single Ti, V, Cr, Mn, Fe, Co, Ni, binary, or multiple metal elements) and [NaO₆] octahedra or prisms^[11a, 20]. In accordance with Delmas' classification rule, based on the local atomic configuration for sodium established by surrounding oxygen and the number of repeating Tm or sodium layers, Na_xTmO₂ can be categorized into O3, O2, P2, and P3 phases. Here, O and P denote octahedral and prismatic structures, respectively, while the numerical value indicates the count of distinct interlayers bordered by various oxide layers. The O3-phase is represented by the range $0.7 \le x \le 1$, with the P2 and P3

phase occurring when x is approximately 0.7 and 0.5, respectively. The original P2 phase transforms into the O2 phase upon extracting a specific amount of Na⁺. Typically, cathodes with the O3 structure and the P2 structure possess a broad interlayer space^[8c, 20]. The broad interlayer space provides numerous sites for the adsorption of H₂O from the surrounding humid environment, contributing to and exacerbating material deterioration. In fact, the air degradation of Na_xTmO₂ exhibits similarities with the degradation observed in high-nickel lithium-based layered cathodes^[18c, 21]. Generally, in a humid environment, the complex interaction between H₂O, CO₂, and Na_xTmO₂ at the surface and bulk levels, leads to a significant loss of active Na⁺ and structural changes^[18c, 22] (**Figure 2a**). Recent advancements in characterization techniques and systematic investigations have clarified and rationalized the connections between the intertwined reactions of Na_xTmO₂ with moisture exposure. These findings provide a clearer understanding of the determining factors influencing structural transformations.

For Na_xTmO₂ with the O3 structure and hygroscopicity, the humidity and oxygen content in ambient conditions result in the spontaneous extraction of Na⁺, oxidation of transition metals, and concurrent transition to sodium-deficient phases^[23]. In detail, Na⁺ within the layer easily undergoes exchange with hydrogen ions by absorbing H₂O from the surrounding environment to form sodium residue salts, such as Na₂O and NaOH. Moreover, the robust hydrophilic properties of NaOH produced on the surface exacerbate the issue, leading to the absorption of a significant amount of water. This further facilitates the exchange of Na⁺ and protons, resulting in the formation of NaHCO₃ and Na₂CO₃ in the presence of CO₂. The formation of these undesired sodium salts not only results in a substantial loss of active Na⁺ but also increases the alkalinity of the material surface, leading to severe implications in the preparation of cathode slurry, which will be explored more deeply later. Subsequently, the oxygen and Na_xTmO₂ continue to interact, resulting in the oxidation of Tm. Additionally, extraction of Na⁺ causes a phase shift from a layered transition metal to disordered structures accompanied with emission of oxygen gas and cracking^[24] (**Figure 2b**). In short, the above process can be described as follows^[17a].

$$NaTmO_2 + xH_2O \rightarrow Na_{1-x}TmO_2 + xNaOH \tag{1}$$

$$NaTmO_2 + xO_2 \to Na_{1-4x}TmO_2 + 2xNa_2O \tag{2}$$

 $NaTmO_2 + xH_2O \rightarrow Na_{1-2x}TmO_2 + xNa_2O + H_2$ (3)

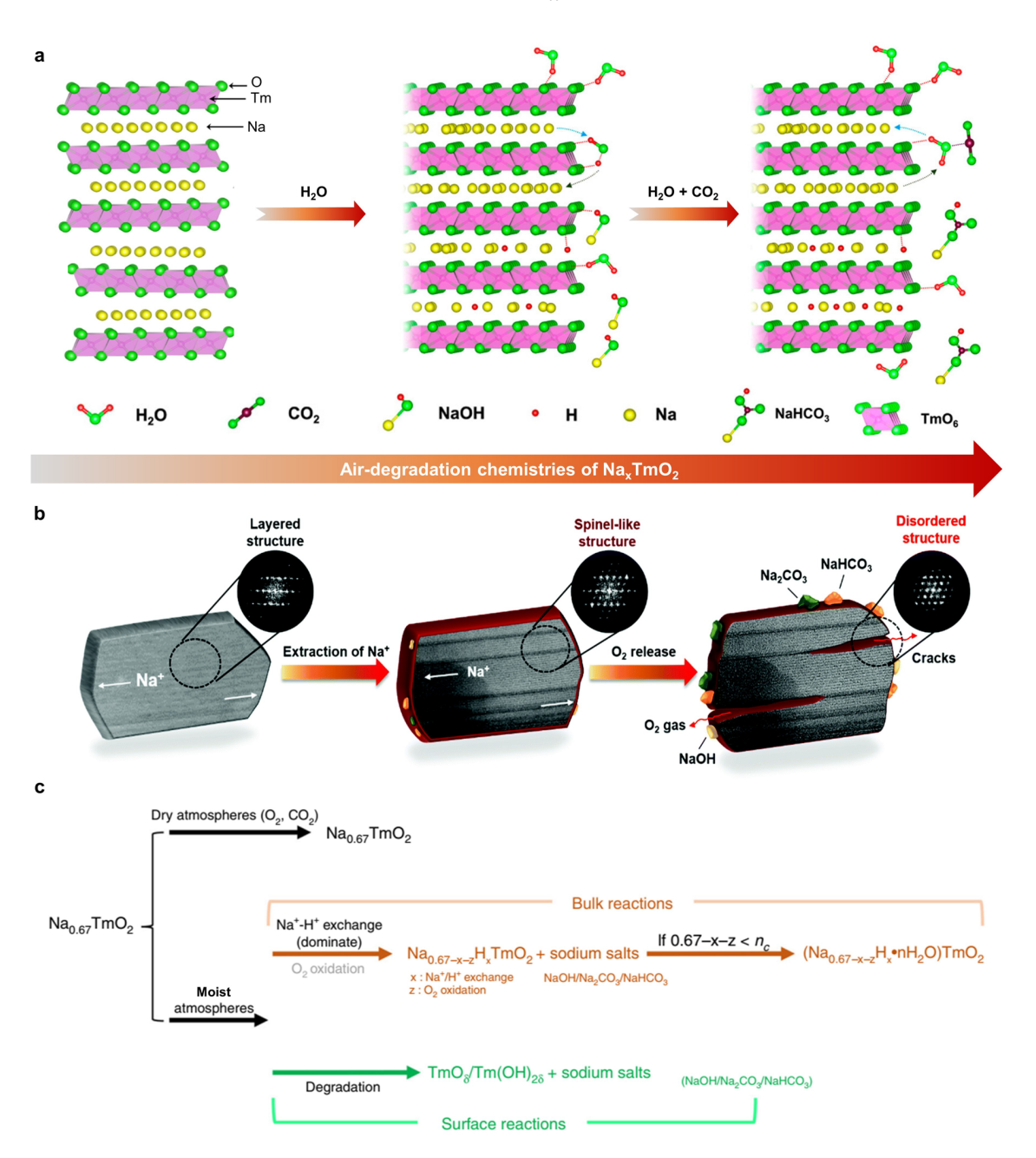


Figure 2. Air degradation chemistries of layered Na_xTmO₂ with O3 and P2 structure. (a) Schematic of air induced degradation process of layered Na_xTmO₂^[18c, 22] (Adapted with permission [REF18c], Copyright 2022, ACS Publisher, Adapted with permission [REF22], Copyright 2020, Springer Nature Publisher). (b) Schematic illustration for the degradation mechanism of air-exposed NaTmO₂ with O3 structure^[24] (Reproduced with permission [REF24], Copyright 2021, Royal Society of Chemistry Publisher). (c) Detailed surface and bulk chemical reactions for the air-exposed Na_{0.67}TmO₂ with P2 structure^[22] (Reproduced with permission [REF22], Copyright 2020, Springer Nature Publisher).

In addition to the degradation process mentioned above, it is observed that H₂O molecules and carbonate ions exhibit a preference for insertion into the interlayers of the P2 structure, facilitated by

the accommodating ability of the larger prismatic sites. When considering Na_{0.67}TmO₂ as an example, it is observed that in its initial stage, the birnessite impurity phase obtained in Na_{0.67}TmO₂ after intercalation of H₂O exhibits structures similar to that of P2-Na_{0.67}TmO₂, except for the expanded interlayer distance. Following additional H₂O insertion, the transformation from the birnessite to the buserite phase is observed with a larger interlayer space^[25]. During this process, the accompanying carbonate molecules can also intercalate into the layered structure. In brief, the above process can be described as follows^[17a, 22] (**Figure 2c**):

$$Na_{0.67}TmO_2 + xH_2O \to Na_{0.67-x}H_xTmO_2 + xNaOH \tag{4}$$

$$3Na_{0.67}TmO_2 + 2xCO_2 + 2xH_2O \rightarrow 3Na_{0.67-x}H_xTmO_2 + xNa_2CO_3 + xNaHCO_3$$
 (5)

$$Na_{0.67-x}H_xTmO_2 + yH_2O \to Na_{0.67-x}H_x(H_2O)_yTmO_2$$
 (6)

$$Na_{0.67}TmO_2 + 1/12CO_3^{2-} \rightarrow 9/8(Na_{16/27}Tm_{8/9}C_{2/27}O_2)$$
 (7)

A recent study reported by Dr. Yong Yang's group provides a comprehensive analysis of the crucial role of Tm in preserving the air stability of Na_xTmO₂, as well as elucidating the associated degradation mechanism^[22]. This research work emphasized the effects of Tm (such as V, Mn, Ru, Ir, Co, Cr, Fe, Ni, and Cu) in terms of their valence state or redox potential evolution on the air-stability of Na_xTmO₂. Take the Mn-based Na_xTmO₂ for example: the air-stability is closely related to the valence state of Mn, following the order of Na_{0.67}Ni²⁺_{0.33}Mn⁴⁺_{0.67}O₂ > Na_{0.67}Zn²⁺_{0.2}Mn^{3.66+}_{0.8}O₂ > Na_{0.67}Zn²⁺_{0.1}Mn^{3.47+}_{0.9}O₂ > Na_{0.67}Al³⁺_{0.1}Mn^{3.37+}_{0.9}O₂ > Na_{0.67}Mn^{3.33+}O₂. Additionally, an empirical rule was suggested to assess the air-stability of Na_xTmO₂. The higher redox potential of Tm, such as Cu²⁺/₃+(\sim 4.05 V), Ni²⁺/₄+(\sim 4.0 V) are demonstrated with enhanced air compatibility compared to that of V³⁺/₄+ (\sim 1.8 V), Mn³⁺/₄+ (\sim 2.35 V), Co³⁺/₄+ (\sim 3.25 V), Fe³⁺/₄+ (\sim 3.25 V) processing low potential.

To summarize, when Na_xTmO₂ is exposed to air, the primary threat comes from hydration or exchange interaction induced by H₂O molecules, leading to the loss of active Na⁺. The presence of CO₂ molecules further intensifies this reaction due to their acidity, giving rise to the formation of sodium salts with strong hygroscopic properties, including NaOH, NaHCO₃, and Na₂CO₃. These side products adversely impact the overall electrochemical performance, causing restricted capacity and a shortened calendar life. Understanding and resolving the chemistries of air-induced degradation are

crucial for advancing the development of Na_xTmO_2 and practical applications of SIBs. In the subsequent sections, we will delve into a comprehensive discussion of the impact of air-induced degradation, covering aspects from the material level to battery manufacturing and overall performance.

3. Effect of air-induced degradation of layered Na_xTmO₂ on manufacturing

6 of SIBs

5

7

8

9

10

11

12

13

14

15

16

17

18

19

20

21

22

23

24

25

26

27

28

As noted above, the air-induced degradation of layered Na_xTmO₂ has multifaceted implications, such as effects towards intrinsic crystal structure^[22, 26], morphology^[18a], slurry preparation^[27], and the overall performance of SIBs^[23b, 28]. This degradation poses challenges that extend beyond mere material deterioration; it intricately intertwines with crucial manufacturing and operation aspects of SIBs (**Figure 3**). Initially, due to the high electropositivity of Na⁺, the interaction of layered Na_xTmO₂ with moisture and carbon dioxide in the air typically initiates the loss of active Na⁺, concomitant with a phase transition. Based on the systematic characterization and analysis enabled by neutron powder diffractions (NPD) and thermogravimetric analysis (TGA)⁴⁵, Manthiram and co-workers revealed that the phase transition of water-treated NaNi_{0.3}Fe_{0.4}Mn_{0.3}O₂ from O3 to hydrated O3 to hydrated P2 and rock-salt phases, as displayed in Figure 3a. Furthermore, Yang and co-workers identified that Na_{0.67}MnO₂, initially characterized by a representative P2 structure with a layer spacing of 5.5 Å, undergoes a transformation into the birnessite structure with a broader interlayer distance of approximately 7.1 Å after exposure to a humid environment (Figure 3b). Following the further insertion of H₂O and an increased interlayer distance of about 9.1 Å, Na_{0.67}MnO₂ ultimately transitions into the buserite phase³⁸. Typically, the P2-phase is considered to be more stable than the P3-phase Na_xTmO₂. This is due to the larger interlayer spacing in P3-phase, which can accommodate not only Na⁺ but also larger molecules like H₂O^[29]. In most P2-phase Na_xTMO₂, only a small portion of Na⁺ is lost with the formation of Na₂CO₃ on the surface. The further formation of Na₂CO₃ can be slowed down under dry air storage. However, in O3-phase Na_xTMO₂, Na loss persists even under dry air storage, which is triggered by the structural transition from O3-phase to a P3-phase^[19b].

Upon exposure to air, the degradation products, NaOH, NaHCO₃, and Na₂CO₃, exhibit gradual growth on the surface of Na_xTmO₂ particles and in the interstitial spaces between adjacent particles,

as displayed in **Figure 3c**. Over time, a thick layer of impurities fully envelops the surfaces of the Na_xTmO₂ particles, rendering the primary particles scarcely visible^[18a]. The surface degradation imposes strict requirements for production, storage, and application, especially in humidity control to avoid the loss of active Na⁺, which would potentially sacrifice the cost advantage of SIBs. Another noteworthy factor is the elevation of surface alkalinity in exposed Na_xTmO₂ and corresponding dehydrofluorination of PVDF (polyvinylidene fluoride) induced by these alkaline substances^[27,30]. This phenomenon significantly impacts the cathode slurry preparation process, as illustrated in **Figure 3d**. Specifically, when processing alkaline Na_xTmO₂ into a slurry, it starts as a pourable ink with flow characteristics, gradually transforming into a gel-like substance over time. This evolution renders inadequate binding and the formation of agglomerated particles in the coating. Additionally, the water absorbed on the surface of Na_xTmO₂ in the N-Methyl-2-pyrrolidone (NMP) slurry induces a bubble effect. Throughout the drying process, the release of both physiosorbed and chemisorbed water from the slurry creates voids or holes on the electrode. This leads to adverse consequences such as electrode cracking, peeling from the current collector, and corrosion of the aluminum current collector^[18a], as shown in the inset of **Figure 3e**.

As discussed, the influence of air exposure introduces various challenges that impact the practical implementation of SIBs. The exchange effect between Na⁺ and protons stands out as a primary issue, causing a notable loss of active Na⁺ and consequently diminishing the reversible capacity of SIBs. Moreover, the accumulation of byproducts on the electrode surfaces leads to an increased resistance to Na⁺ migration, elevating the polarization of SIBs and constraining their practical high-rate capability and lifespan^[23b, 28] (**Figure 3d**). Additionally, the absorption of H₂O not only leads to the production of poor-quality electrodes but also initiates the severe decomposition of the organic-based electrolytes, giving rise to the generation of toxic HF gas. This HF gas, in turn, exacerbates the situation by further etching the surface and bulk of Na_xTmO₂, leading to the production of additional H₂O^[11c, 23b, 31]. This dual effect not only compromises battery stability but also poses a threat to battery safety, thereby reducing the overall lifespan of the SIBs. Consequently, the inherent hygroscopic nature of Na_xTmO₂ poses challenges during the manufacturing and storage processes of the materials and electrodes. These challenges add complexity to the production of practical SIBs and contribute to increased costs.

- 1 Therefore, improving air stability is crucial for preserving the economic viability and cost-
- 2 effectiveness of SIBs.

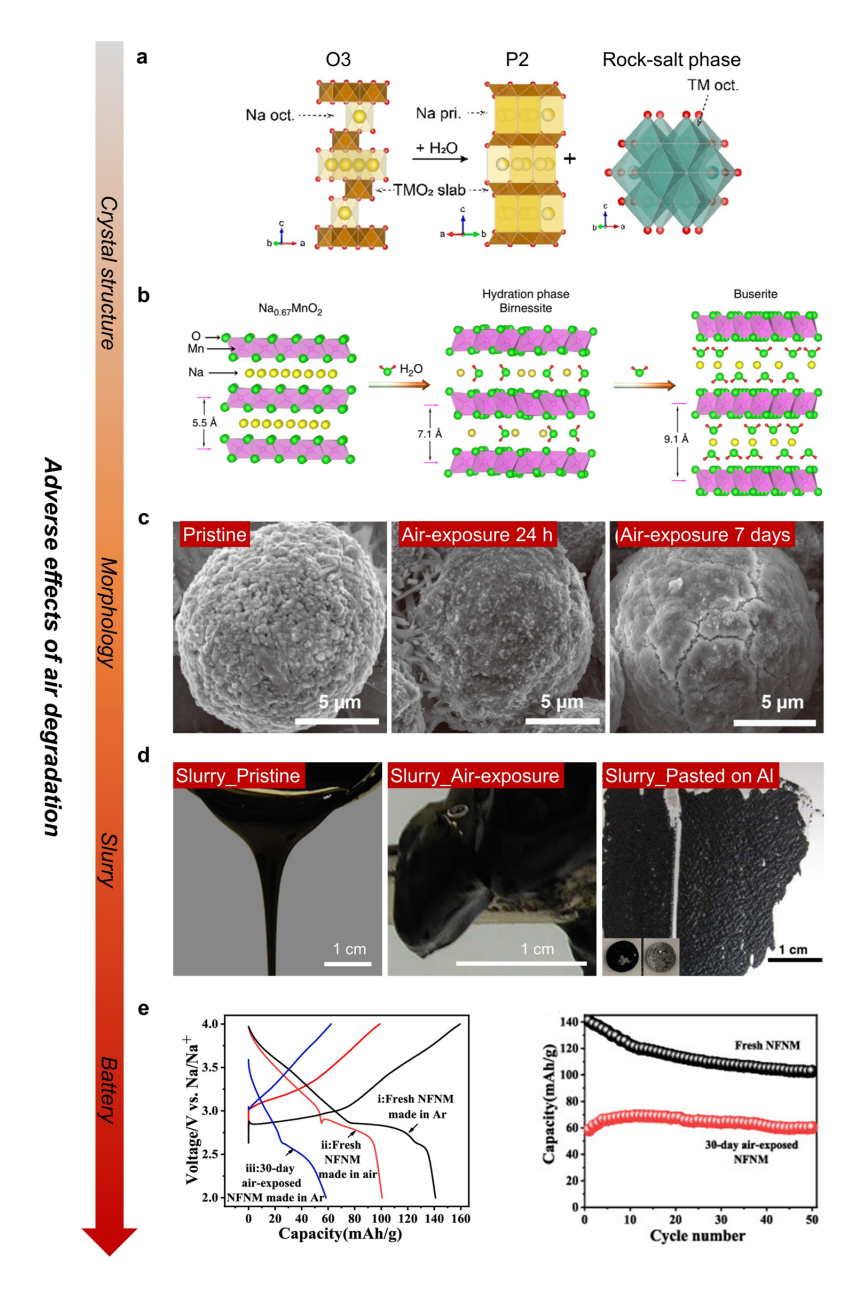


Fig. 3. Adverse effects of air degradation on Na_xTmO₂ cathodes and batteries. (a) Schematic of air degradation induced structure transition of layered Na_xTmO₂ with O3 structure^[26] (Reproduced with permission [REF26], Copyright 2019, ACS Publisher). (b) Schematic of air degradation induced structure transition of layered Na_xTmO₂ with P2 structure^[22] (Reproduced with permission [REF22], Copyright 2020, Springer Nature Publisher). (c) Morphology evolution of the Na_xTmO₂ during air exposure^[18a] (Reproduced with permission [REF18a], Copyright 2018, ACS Publisher). (d) Slurry evolution during air exposure^[27] (Reproduced with permission [REF27], Copyright 2022, Elsevier Publisher). Inset: Cathode electrode after being exposed to air^[18a] (Reproduced with permission [REF18a], Copyright 2018, ACS Publisher). (e) Comparison of electrochemical performance of pristine and air-exposed Na_xTmO₂ cathodes^[28] (Reproduced with permission [REF28], Copyright 2021, ACS Publisher).

4. Improving strategies for air sensitive layered Na_xTmO₂

4.1. Surface protective coating

Surface modification of the cathodes using coating techniques has been widely employed to enhance air-stability and electrochemical performance by improving material conductivity and stabilizing the physical structure^[32]. Numerous studies are dedicated to exploring the application of a durable coating layer onto the surface of Na_xTmO₂ as a practical and scalable approach to mitigate its hygroscopic attraction towards ambient moisture, thereby enhancing their stability and longevity^[33]. Recent studies have revealed that a series of materials such as carbon^[34], metal oxides^[18a, 35], metal phosphates^[36], and the Na super ionic conductor (NASICON, Na_{1+x}Zr₂Si_xP_{3-x}O₁₂, 0 < x < 3)^[37] serve as effective protective coating layers. These introduced isolation barrier layers offer robust protection by effectively preventing the exchange of Na⁺ and protons as well as the erosion of H₂O and CO₂. In addition to its primary role as a barrier, the coating layer on Na_xTmO₂ can minimize adverse reactions between the cathode and the organic electrolyte. It also helps suppress lattice distortion caused by the dissolution of Tm ions into the organic electrolyte during charging, maintaining structure stability and providing considerable reversible capacity.

Utilizing carbon-based materials and metal oxides as non-ionic conductive layers, commonly utilized as a cladding material in commercial coating modifications for cathodes^[38], are renowned for their exceptional thermal stability and environmental compatibility. These properties make it an ideal choice for protective coatings, especially in applications where durability and chemical resistance are crucial. Specifically, Myung and co-workers proposed a novel emulsion method for creating a thin but durable carbon layer with a thickness of ~10 nm on the surface of NaCrO₂ (**Figure 4a**), which effectively suppressed moisture uptake due to the hydrophobic nature of the carbon^[34]. Consequently, the crystal lattice of carbon-coated NaCrO₂ (C@NaCrO₂) remained intact and unchanged, even after an extended exposure to air for 48 hours, highlighting a marked contrast to the behavior of pristine NaCrO₂. In comparison, the latter demonstrated significant phase separation into a sodium-deficient phase (Na_xCrO₂) and NaOH, occurring rapidly upon even a short-term exposure to atmospheric conditions.

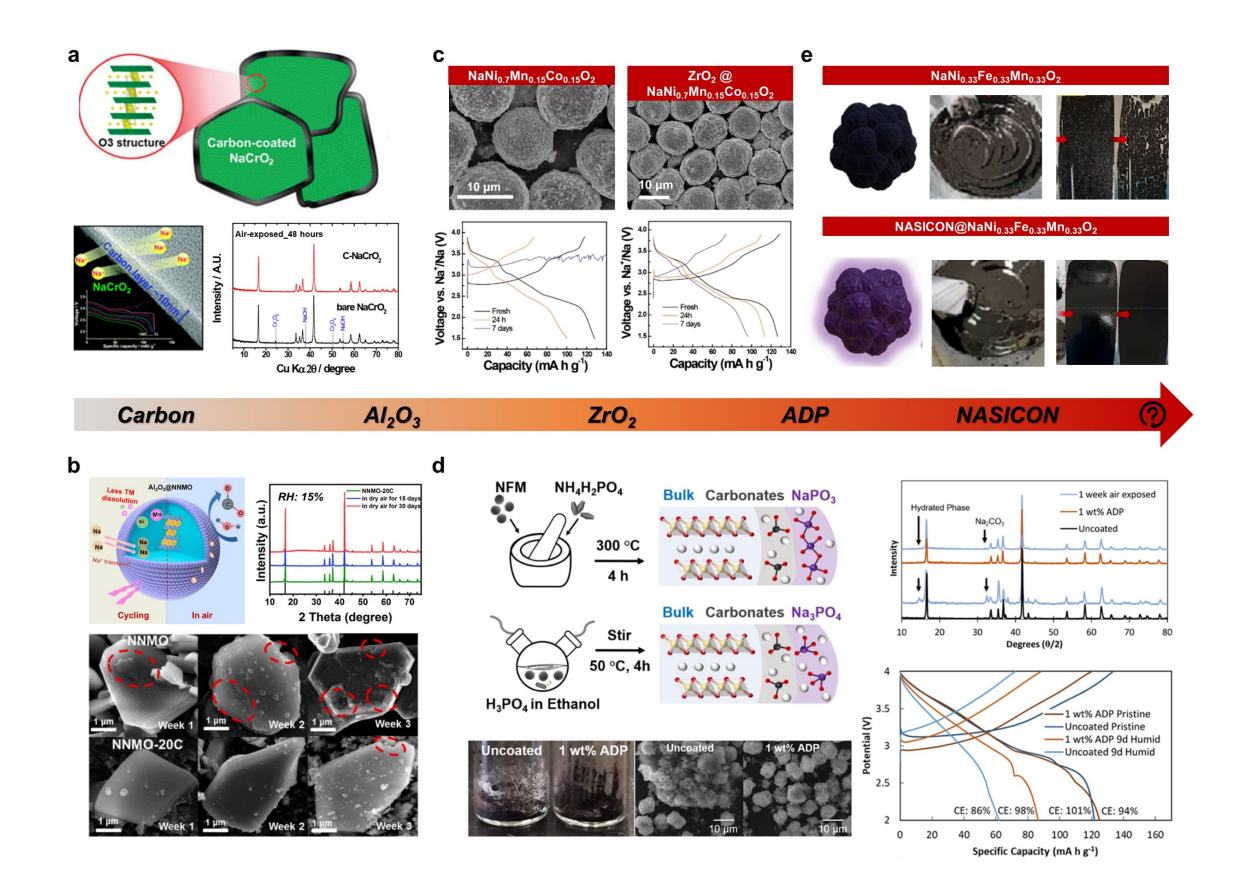


Figure 4. Protective surface coating layer strategies for enhancing air exposure stability. (a) Schematic figure of carbon-based coating layer on the surface of NaCrO₂, TEM image for carbon-coated NaCrO₂, and XRD comparison for bare and carbon-coated NaCrO₂^[34] (Reproduced with permission [REF34], Copyright 2015, Royal Society of Chemistry Publisher). (b) Schematic illustration of the advantages for the Al₂O₃-surface modificationNaNi_{0.6}Co_{0.2}Mn_{0.2}O₂, XRD evolution for corresponding sample exposed to an atmosphere with a humidity of 15%^[35a] (Reproduced with permission [REF35a], Copyright 2021, Elsevier Publisher). (c) SEM and electrochemical performance comparison for bare and ZrO₂-based coated NaNi_{0.7}Co_{0.15}Mn_{0.15}O₂^[18a] (Reproduced with permission [REF18a] Copyright 2018, ACS Publisher). (d) Illustration for Na₃PO₄-based coating method, optical photos and SEM image comparison for uncoated and coated NaNi_{0.3}Fe_{0.4}Mn_{0.3}O₂^[36] (Reproduced with permission [REF36], Copyright 2021, ACS Publisher). (e) Illustration and optical images for pristine and Na₃Zr₂Si₂PO₁₂-coated NaNi_{0.33}Fe_{0.33}Mn_{0.33}O₂^[37] (Reproduced with permission [REF37], Copyright 2023, Elsevier Publisher).

Bai and co-workers successfully utilized the rising technology for surface decoration with the atomic layer deposition (ALD) technique, to encapsulate NaNi_{0.5}Mn_{0.5}O₂ (NNMO) with an Al₂O₃ layer^[35a], as depicted in **Figure 4b**. When subjected to a dry air environment (humidity of 15%) for durations of 15 and 30 days, the Al₂O₃-coated NNMO (Al₂O₃@NNMO) exhibited no signs of structural degradation or surface impurities. In contrast, the pristine NNMO showed severe surface corrosion and significant structure degradation over aging time, a phenomenon markedly less pronounced in the Al₂O₃@NNMO. These improvements indicated the effectiveness of Al₂O₃ in suppressing the intrinsic reactions between NNMO and atmospheric H₂O and CO₂, leading to a significant reduction in the

formation of detrimental impurities, ultimately enhancing the chemical stability. Analogously, Manthiram and co-workers demonstrated that the air stability of NaNi_{0.7}Co_{0.15}Mn_{0.15}O₂ could be significantly enhanced by modifying it with a ZrO₂ layer^[18a], along with improved electrochemical performance (**Figure 4c**). After 24 hours of air exposure, bare NaNi_{0.70}Mn_{0.15}Co_{0.15}O₂ exhibited a decrease in electrochemical performance, with its discharge capacity reduced to 100 mAh g⁻¹. Prolonged exposure for 7 days led to an abnormally high charge capacity, marked by a prolonged charge plateau at 3.4 V. This phenomenon is attributed to the decomposition of sodium carbonates and reactions between the electrolytes and residual sodium species, indicating significant degradation impacts from air exposure. Conversely, ZrO₂@NaNi_{0.70}Mn_{0.15}Co_{0.15}O₂ demonstrated improved durability against air exposure. It maintained notable discharge capacities of 113 and 96 mAh g⁻¹ after similar periods of air exposure, corresponding to 90% and 76% retention of its original capacity, respectively. This indicates that the ZrO₂ coating effectively retards surface and structural degradation, significantly enhancing the stability and performance of the cathode material under air-exposed conditions.

1

2

3

4

5

6

7

8

9

10

11

12

13

14

15

16

17

18

19

20

21

22

23

24

25

26

27

28

29

Compared to non-ion conducting layers that tend to increase charge transfer resistance at the surface/interface, using coatings made of stable ionic conductive materials with high conductivity is emerging as a promising alternative for improving air-stability as well as minimizing resistance. Phosphorus-based materials^[36, 39] are proposed as a practical and scalable protective layer for Na_xTmO₂, attributed to their high abundance and cost-effectiveness. Additionally, sodium phosphates can theoretically form by reacting with residual sodium hydroxide and carbonate species on the surface of Na_xTmO₂, potentially neutralizing harmful residues. Manthiram and co-workers utilized the simple grinding method to apply NaPO₃ coatings on NaNi_{0.3}Fe_{0.4}Mn_{0.3}O₂, effectively shielding the material from moisture-related reactions in the air (Figure 4d), maintaining a high capacity and initial coulombic efficiency of the exposed cathode^[36]. Following water exposure and vacuum heating, bare $NaNi_{0.3}Fe_{0.4}Mn_{0.3}O_2$ experienced sodium leaching residue formation. unlike and ADP@NaNi_{0.3}Fe_{0.4}Mn_{0.3}O₂, which maintained its original particle state. XRD analysis also indicated that ADP@NaNi_{0.3}Fe_{0.4}Mn_{0.3}O₂ maintained strong peak intensity after air exposure, with no hydrated phase and minimal peak shifts. Upon exposure to humid air, the sodium polyphosphate, acted as a water scavenger, converting into hydrated Na₃PO₄ and protecting the bulk layered structure^[36].

Furthermore, Na-containing solid electrolyte candidates are frequently regarded as potential coating layers owing to their high Na-ion conductivity and chemical stability. Motivated by this, Choi and coworkers developed a stable and highly conductive Na₃Zr₂Si₂PO₁₂ (NASICON) coating on NaNi_{0.33}Fe_{0.33}Mn_{0.33}O₂^[37]. Formed using a pre-coating method, this moisture-resistant layer efficiently protects the cathode from humid environments (**Figure 4e**). NASICON@NaNi_{0.33}Fe_{0.33}Mn_{0.33}O₂ effectively maintained its electrode casting quality after humidity exposure by preventing the formation of alkaline products like NaOH and Na₂CO₃^[37]. Conversely, the uncoated NaNi_{0.33}Fe_{0.33}Mn_{0.33}O₂ electrodes faced detachment from the current collector post-casting, an issue attributed to slurry gelation induced by these alkaline products. After 100 cycles, the difference in capacity retention between the NASICON@NaNi_{0.33}Fe_{0.33}Mn_{0.33}O₂ and the unmodified NaNi_{0.33}Fe_{0.33}Mn_{0.33}O₂ was significant. The NASICON-coated cathode retained 74.06% of its original capacity, whereas the unmodified cathode retained only 41.21%. This substantial gap highlights the effectiveness of NASICON in enhancing the air stability of NaNi_{0.33}Fe_{0.33}Mn_{0.33}O₂.

A protective surface coating is crucial for shielding Na_xTmO_2 from direct contact with ambient H_2O and $CO_2^{[18a, 34-37]}$. Although these methods are effective in reducing exposure, thereby reducing the formation of surface impurities and slowing the alteration of the bulk phase structure, they are not an ultimate solution. Additionally, the introduction of a coating layer, an inactive component for batteries, can increase the barrier to ion migration and electrolyte percolation, potentially compromising the ion migration, charge transfer process at the interface and overall energy density. Therefore, one of the key challenges for the future is to develop innovative coating layers specifically designed to fully prevent air-induced degradation of Na_xTmO_2 without sacrificing performance.

4.2. Surface chemistry and structure reconstruction

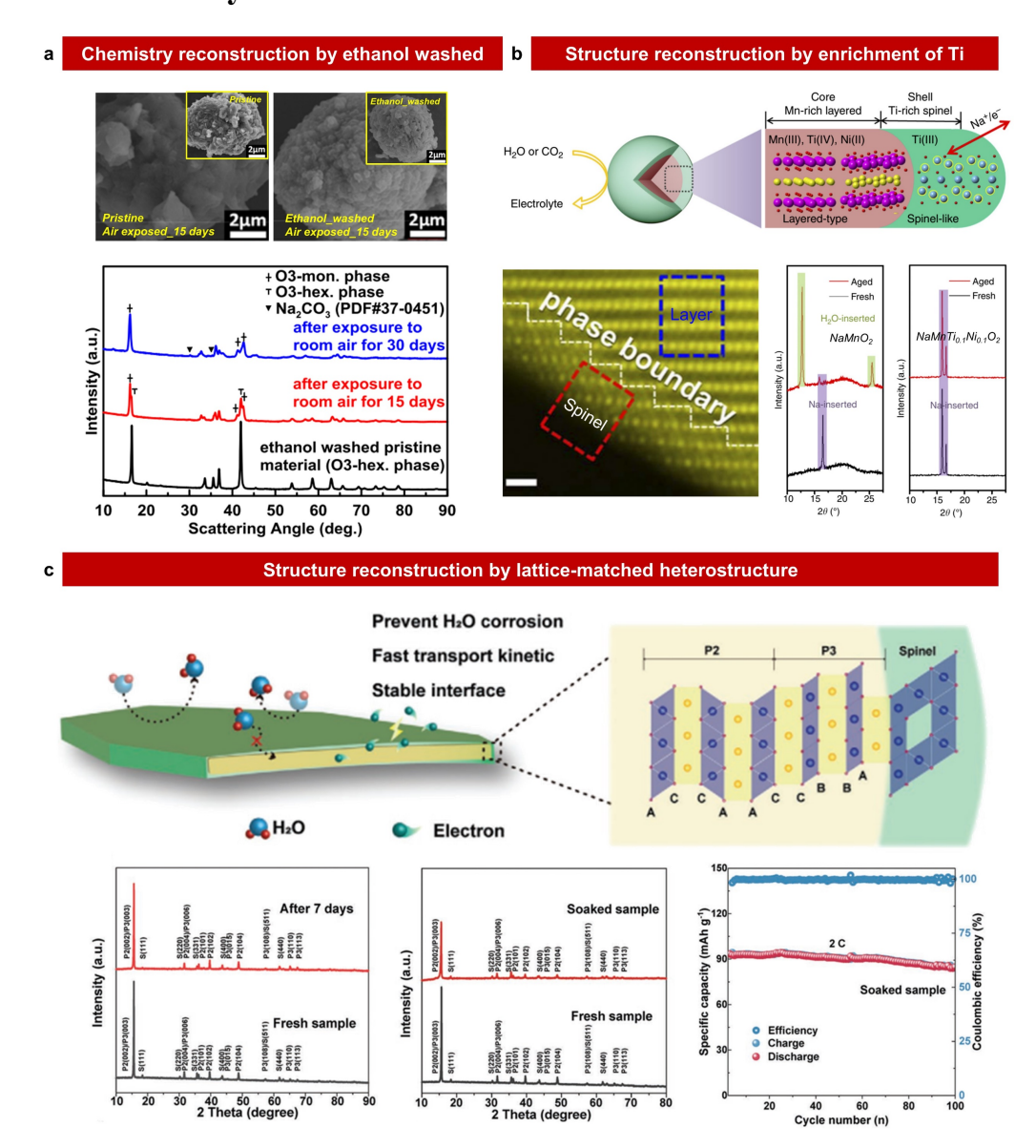


Figure 5. Surface chemistries and structure reconstruction to improve air-stability of Na_xTmO₂. (a) SEM images and corresponding XRD data for cathodes pre and post wash process^[40] (Reproduced with permission [REF40], Copyright 2018, ACS Publisher). (b) Schematic for spinel-structured titanium-enriched interface protective strategy, STEM image for typical NaMnTi_{0.1}Ni_{0.1}O₂ bulk structure (scale bar: 0.5 nm), and XRD evolution data for NaMnO₂ and NaMnTi_{0.1}Ni_{0.1}O₂ samples^[41] (Reproduced with permission [REF41], Copyright 2017, Spinger Nature Publisher). (c) Illustration of the P2/P3@ Na_{0.5}Mg_{0.2}Co_{0.15}Mn_{0.65}O₂ cathode material, XRD patterns of fresh samples before and after air exposure, and XRD patterns comparing fresh samples with samples post-soaking treatment^[42] (Reproduced with permission [REF42], Copyright 2023, Wiley Publisher).

Air exposure triggers the degradation of Na_xTmO_2 starting at the surface where interactions with environmental elements initiate the deterioration process. To fundamentally address the air instability of Na_xTmO_2 , innovative advancements in surface chemistry and structural reconstruction are essential.

Such approaches are expected to provide robust solutions by modifying the interactions of cathodes with environmental factors on a molecular level, thereby enhancing intrinsic stability.

3

4

5

6

7

8

9

10

11

12

13

14

15

16

17

18

19

20

21

22

23

24

25

26

27

28

29

During the sintering of Na_xTmO₂, an excess of sodium precursors is often used to offset sodium loss. This can inevitably result in sodium residues in the final product, which are electrochemically inactive and hygroscopic. Therefore, removing these residues could be crucial to ensure their effectiveness and stability. Reconstructing the surface chemistries enabled by a simple washing process to remove the surface impurity leads to better cycling and stronger resistance to ambient H₂O and CO₂, which was confirmed in cathodes of lithium-ion batteries^[43]. Obrovac and co-workers proposed ethanol washing as an effective method for removing sodium residues from the surface of NaNi_{0.5}Mn_{0.5}O₂^[40]. As previously discussed, the thickness of hygroscopic sodium residues increases due to the repeated cycles of desodiation and water absorption. Eliminating these surface impurities leads to reduced hystereses and higher reversible capacities. Ethanol-washed NaNi_{0.5}Mn_{0.5}O₂ samples exhibit a much thinner coating after air exposure, allowing the primary particles to remain distinguishable, while pristine NaNi_{0.5}Mn_{0.5}O₂ particles undergo significant surface changes, getting completely coated by a substance that also fills the gaps between primary particles, rendering them indistinguishable. As a result, the ethanol-washed NaNi_{0.5}Mn_{0.5}O₂ demonstrates higher capacity compared to its pristine counterpart, mainly due to the reduced hysteresis. This contrast highlights the effectiveness of ethanol washing in maintaining particle integrity and reducing surface alteration due to air exposure. Crucially, this method not only significantly boosts the stability upon air exposure but also has an impact on the bulk cathode material of air-sensitive substances, as illustrated in Figure 5a. The rinsing method for Na_xTmO₂ has its limitations due to solvent nature and compatibility issues with the Na_xTmO₂. Additionally, while removing surface impurities can alleviate airborne degradation, it does not prevent active Na⁺ loss in the bulk phase, indicating a need for more comprehensive solutions to address these challenges.

Unlike surface chemistry reconstruction by washing, structural reconstruction, facilitated by the spontaneous formation of protective surface oxide layers during sintering without additional processing, is highly anticipated to enhance the intrinsic air stability^[41-42, 44]. Zhou and co-workers developed an atomic-scale interface with spinel-like titanium (III) oxides for NaMnO₂ surface reconstruction^[41], which effectively hampers water intercalation. After a 3-day air exposure, structural

analysis of NaMnTi_{0.1}Ni_{0.1}O₂ showed a diffraction pattern consistent with the pristine material and no new phases, underscoring the protective effectiveness of the titanium (III) oxide interface. The resistance to water intercalation can likely be ascribed to its spinel-like structure, acting as an effective barrier against water penetration (Figure 5b). Other than that, Zhou and co-workers also proposed a novel approach for manganese-based oxide cathodes involving passivated Tm-rich and Na-free nanoscale surface reconstruction^[44], effectively preventing surface interactions with ambient surroundings. Remarkably, this modification resulted in exceptional air stability. The treated cathodes maintained their complete crystal structure and electrochemical performance even after 60 days of exposure to humid air or 5 days of immersion in water. The electrochemical performance of Na_{2.3}Cu_{1.1}Mn₂O_{7-δ} after prolonged exposure to humid conditions is also remarkable. Even after 60 days in such an environment, it delivers exceptional cycling performance, maintaining a high level of capacity retention (95.8%) after 1000 cycles. This endurance showcases its robustness and reliability, marking it as a promising candidate for long-term energy storage solutions. Other than that, Xiao and co-workers implemented in-situ spinel interfacial reconstruction on the Na_{0.5}Mg_{0.2}Co_{0.15}Mn_{0.65}O₂ surface via lattice-matched engineering, providing an effective protective layer that reduces direct contact with H₂O and enhances air stability^[42]. The reconstructed Na_{0.5}Mg_{0.2}Co_{0.15}Mn_{0.65}O₂ demonstrated remarkable stability after exposure to the ambient environment and even after water immersion, showing negligible shifts in its diffraction patterns compared to the original. This material also maintained excellent electrochemical performance, with a high discharge capacity of 84.7 mAh g⁻¹ at 2 C rate, underscoring its potential for robust and efficient energy storage applications. (Figure 5c).

1

2

3

4

5

6

7

8

9

10

11

12

13

14

15

16

17

18

19

20

21

22

23

24

25

26

In summary, the air instability of Na_xTmO₂ can be mitigated through advanced surface chemistry and structural reconstruction. This involves the removal of surface impurities and the implementation of atomic-scale interfaces and lattice-matched engineering. These strategies lead to significant improvements in air stability and the preservation of electrochemical functionality, even in prolonged humid conditions.

4.3. Crystal structure engineering by heteroatom substitution

4.3.1. Superlattice ordering of Tm layer

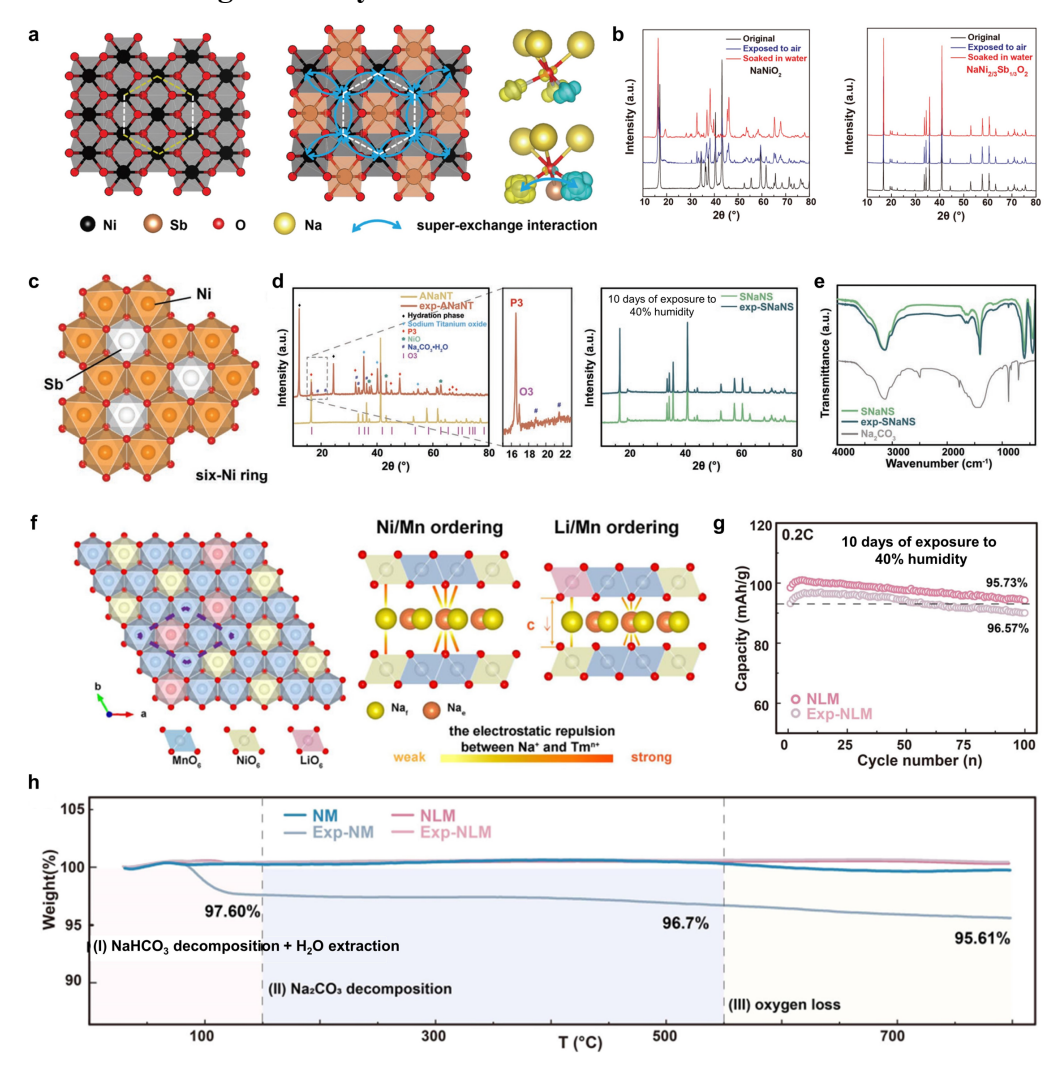


Figure 6. Enhanced air stability of Na_x**TmO**₂ by Superlattice-effect. (a-b) Comparison of bond length of NaNiO₂ and NaNi_{2/3}Sb_{1/3}O₂ and corresponding X-ray diffraction patterns of as-synthesized, air-exposed, and water soaked NaNiO₂ and NaNi_{2/3}Sb_{1/3}O₂^[47] (Reproduced with permission [REF47], Copyright 2019, Wiley Publisher). (**c-e**) The structure diagram of symmetrical O3-NaNi_{2/3}Sb_{1/3}O₂ with six-Ni ring, X-ray diffraction patterns, and Fourier-transform infrared spectroscopy of as-synthesized and air-exposed NaNiO₂ and O3-NaNi_{2/3}Sb_{1/3}O₂^[48] (Reproduced with permission [REF48], Copyright 2023, Wiley Publisher). (**f-h**) Structure diagram of Na_{0.67}Ni_{0.33}Li_{0.10}Mn_{0.57}O₂, corresponding cycling performance and thermogravimetric analysis of assynthesized, air-exposed Na_{0.67}Ni_{0.33}Li_{0.10}Mn_{0.57}O₂^[49] (Reproduced with permission [REF49], Copyright 2023, Wiley Publisher).

Crystal structure optimization is a foundational approach to adjusting physical and chemical properties by manipulating the crystal structure or local chemical environment at the atomic level. In the case of Na_xTmO_2 , its observed poor structural stability, particularly in the context of multiple phase evolution, is attributed to two main factors: the ordering and disordering of cations, and the lateral

movement of Tm layers^[45]. Heteroatom substitution in Na_xTmO₂ plays a crucial role in the optimization process, effectively modifying interlayer spacing, bonding energy, the interaction between Tm layer and sodium layer, and local ordering/disordering^[46]. This results in improved electrochemical performance and intrinsic air-stability.

5

6

7

8

9

10

11

12

13

14

15

16

17

18

19

20

21

22

23

24

25

26

27

28

29

Back in 2001, Dahn at al. suggested that the presence of Ni cation ordering in P2-Na_{2/3}Ni_{1/3}Mn_{2/3}O₂ can format $\sqrt{3}a \times \sqrt{3}a$ hexagonal superlattice in the Tm layers, which strengthens the interlayer interaction and prevents water intercalation³³. Based on this, Guo and co-workers tackled the issue of air-exposure degradation by choosing two ions with significantly distinct M-O bond energies^[47]. The substitution of one-third of the Ni with Sb in NaNiO₂ leads to the formation of a superlattice of ordered Ni₆-rings in the Tm layers of the model compound NaNi_{2/3}Sb_{1/3}O₂. This alteration induces superexchange interactions, resulting in a symmetric atomic configuration, averaged bond length, and degenerate electronic orbitals within the layered oxides, based on the atomic and electronic structure analyses (Figure 6a, b). The Ni₆-rings, formed through Ni/Sb ordering and characterized by superexchange interactions, play a pivotal role in significantly enhancing the air and phase stability of pristine NaNiO₂. XRD results revealed a gradual weakening and disappearance of the characteristic peaks of (111) for as-synthesized, air-exposed, and water-soaked NaNiO₂, which can be attributed to the exchange of Na⁺ and protons, inducing a change in the O-O layer spacing. In contrast, there was no change of intensity or shift of peaks observed in the XRD patterns of air-exposed and water-soaked NaNi_{2/3}Sb_{1/3}O₂ compared to the as-synthesized one, demonstrating the enhancement of air stability enabled by the superlattice effect.

Following this line of thought, Yao and co-workers devised a strategy to construct stable Tm layers. This approach centers on creating a highly symmetrical six-Tm ring structure within O3-NaNi_{2/3}Sb_{1/3}O₂^[48]. Notably, this methodology is adaptable and can be extended to include P2-type layered oxides as well. The overall symmetrical Tm layer structure in this strategy raises the energy barrier required for the aging reaction between the material and air. Aging experiments revealed an apparent structural change with the formation of the Na₂CO₃ phase in asymmetrical NaNi_{2/3}Ti_{1/3}O₂. In contrast, symmetrical O3-NaNi_{2/3}Sb_{1/3}O₂ preserved the original XRD pattern without the formation of any new peaks, demonstrating the enhanced structural stability and consequently impeding ambient air corrosion (**Figure 6c-e**). Subsequently, Yao and co-workers introduced an innovative strategy by

proposing a novel cation ordering approach. This method aims to concurrently establish the coexistence of Na⁺ disordering with ordered Tm arrangements, thereby enhancing interactions between Tm layers and effectively blocking the incorporation of water molecules from the air^[49]. As a result, Na_{0.67}Ni_{0.33}Li_{0.10}Mn_{0.57}O₂, when exposed to air for 10 days at 40% humidity, exhibited remarkable electrochemical performance. It maintained 94.72% of its capacity compared to the pristine cathode, even after 100 cycles. Furthermore, the absence of noticeable weight losses in Na_{0.67}Ni_{0.33}Li_{0.10}Mn_{0.57}O₂ throughout the entire heating process directly indicates a substantial improvement in both air stability and lattice stability (**Figure 6f-h**).

In short, based on the arrangement of the highly symmetric transition metal layer's structure, the superlattice ordering shows effectiveness for air stabilization of both O3 and P2-type Na_xTmO₂. Nonetheless, due to the pronounced ion interaction within the alkali metal layer and the charge ordering in Tm layers, the superlattice structure typically present in Tm layers often induces the formation of Na⁺/vacancy ordering the sodium layer. This significantly influences its structural stability during Na⁺ extraction and insertion, leading to the formation of an ordered superstructure, which can cause considerable volume changes and potentially trigger structural destruction and phase transition^[45b, 50]. This phenomenon has the potential to hinder the transport kinetics of Na⁺, leading to a subsequent compromise in rate performance^[18b, 46c].

4.3.2. Conventional Heteroatom Substitution of Tm and Sodium Sites

2

3

4

5

6

7

8

9

10

11

12

13

14

15

16

17

18

19

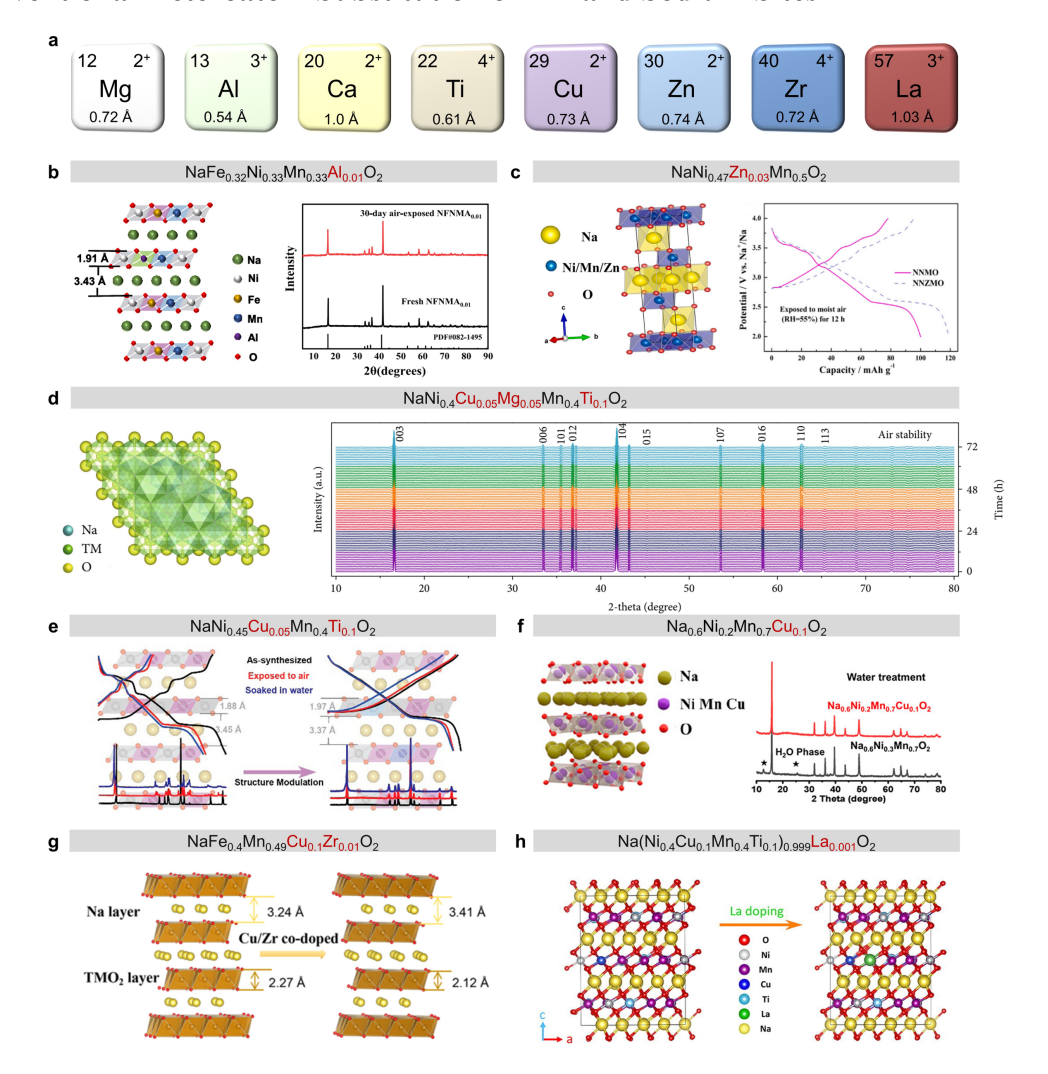


Figure 7. Conventional heteroatoms substitution strategy for air-stable layered Na_xTmO₂. (a) Heteroatoms for doping modification of layered Na_xTmO₂. The upper left, upper right, and lower information is the atomic number, valence, and ionic radius, respectively. (b) Structure schematic of Al-substitution for O3-NaFe_{0.33}Ni_{0.33}Mn_{0.33}O₂ and corresponding X-ray diffraction patterns of fresh and 30-day air-exposed NaFe_{0.32}Ni_{0.33}Mn_{0.33}Al_{0.01}O₂^[28] (Reproduced with permission [REF28], Copyright 2021, ACS Publisher). (c) Structure schematic of Zn-substitution for O3-NaNi_{0.47}Zn_{0.03}Mn_{0.5}O₂ and electrochemical performance comparison of air-exposed O3-NaNi_{0.5}Mn_{0.5}O₂ and O3-NaNi_{0.47}Zn_{0.03}Mn_{0.5}O₂^[51] (Reproduced with permission [REF51], Copyright 2021, Elsevier Publisher). (d) Structure schematic of co-substitution of Cu, Mg, and Ti for NaNi_{0.5}Mn_{0.5}O₂ and in-situ X-ray diffraction patterns of air-exposed NaNi_{0.4}Cu_{0.05}Mg_{0.05}Mn_{0.4}Ti_{0.1}O₂^[52] (Reproduced with permission [REF52], Copyright 2020, AAAS Publisher). (e) Structure schematic of cosubstitution of Cu and Ti for NaNi_{0.5}Mn_{0.5}O₂ and corresponding electrochemical performance and X-ray diffraction patterns^[23a] (Reproduced with permission [REF23a], Copyright 2020, ACS Publisher). (f) Structure schematic of P2-Na_{0.6}Ni_{0.2}Mn_{0.7}Cu_{0.1}O₂ and corresponding X-ray diffraction patterns of water-treated P2-Na_{0.6}Ni_{0.3}Mn_{0.7}O₂ and Na_{0.6}Ni_{0.2}Mn_{0.7}Cu_{0.1}O₂^[53] (Reproduced with permission [REF53], Copyright 2017, ACS Publisher). (g) Structure schematic of co-substitution of Cu and Zr for NaFe_{0.5}Mn_{0.5}O₂^[54] (Reproduced with permission [REF54], Copyright 2021, ACS Publisher). (h) Structure schematic of Co-substitution of Cu, Ti, and La for NaNi_{0.5}Mn_{0.5}O₂^[55] (Reproduced with permission [REF55], Copyright 2022, Elsevier Publisher).

Beyond the construction of superlattices, research has shown that the introduction of some trace amounts of heteroatoms at Tm sites significantly enhances the intrinsic air stability of Na_xTmO₂. This enhancement is attributed to changes in sodium content, bonding energy of Na-O and Tm-O, Tm valences, interfacial chemical properties, and interlayer spacing. Heteroatoms commonly used for such doping include Mg, Al, Ti, Cu, Zn, Zr, and La, either individually or in combination, as detailed in **Figure 7a**.

1

2

3

4

5

6

7

8

9

10

11

12

13

14

15

16

17

18

19

20

21

22

23

24

25

26

27

28

29

To restrain the air-induced degradation of O3-NaFe_{0.33}Ni_{0.33}Mn_{0.33}O₂, Zhao and co-workers used the co-precipitation method to introduce a trace amount of Al to replace Fe inserting into the NaFe_{0.33}Ni_{0.33}Mn_{0.33}O₂ crystal lattice (Figure 7b), due to the similar ionic radius of Al³⁺ (53.5 pm) vs. Fe³⁺ (55.0 pm)^[28]. After 30 days of air exposure, NaFe_{0.33}Ni_{0.33}Mn_{0.33}O₂ experienced a significant decline in crystallinity, indicating a severe deterioration of its O3 structure. The obtained NaFe_{0.32}Ni_{0.33}Mn_{0.33}Al_{0.01}O₂ maintained its original crystal structure even after exposure to air for 30 days, attributed to a stronger bonding energy of Al-O (512 kJ mol⁻¹) compared to Fe-O (409 kJ mol⁻¹). The robust bonding effect plays a crucial role in stabilizing the crystal structure, effectively suppressing the migration of Na⁺ from the bulk to the surface. This phenomenon helps avoid unfavorable chemical reactions with CO₂ and moisture in the air. After 30 days of air exposure, both NaFe_{0.33}Ni_{0.33}Mn_{0.33}O₂ and its modified counterpart NaFe_{0.32}Ni_{0.33}Mn_{0.33}Al_{0.01}O₂ showed varying degrees of capacity retention. The former could deliver a capacity of around 60 mAh g⁻¹, while the latter exhibited a higher capacity of approximately 130 mAh g⁻¹. This difference in performance underscores the impact of air exposure on these materials and the potential benefit of compositional modifications by trace amount of heteroatom doping. Successful doping of Zn into the Ni-site of NaNi_{0.5}Mn_{0.5}O₂ was also achieved using the traditional solid-state method [51]. Upon air exposure, the modified NaNi_{0.47}Zn_{0.03}Mn_{0.5}O₂ exhibited excellent charge and discharge capacities (120 mAh g⁻¹), alongside stable coulombic efficiency and cyclic stability, particularly in comparison to the air-exposed undoped NaNi_{0.5}Mn_{0.5}O₂ (Figure 7c). These results underscore the effectiveness of heteroatom doping as a strategy to enhance air-stability of Na_xTmO₂.

Furthermore, the integration of a high potential redox couple of copper(II)/copper(III) (Cu^{2+}/Cu^{3+} , ~3.8 V) into the composition of layered Na_xTmO_2 , applicable in both O-type and P-type resulted in outstanding electrochemical performance and enhanced air stability. Numerous research groups have

dedicated substantial efforts to the ongoing development and uncovering of the stabilization 1 mechanism of Cu-based Na_xTmO₂ cathodes. Guo and co-workers suggested that synergistic effects 2 arising from multielement chemical substitution could be the key to developing air-stable O3-type 3 Na_xTmO₂^[52]. NaNi_{0.4}Cu_{0.05}Mg_{0.05}Mn_{0.4}Ti_{0.1}O₂ was synthesized by introducing Cu, Mg, and Ti to 4 partially replace Ni and Mn. With a 3-day air exposure, the in-situ XRD patterns of 5 NaNi_{0.4}Cu_{0.05}Mg_{0.05}Mn_{0.4}Ti_{0.1}O₂ revealed that no additional peaks were observed beyond the O3-type 6 phase, and the intensity of the various peaks remained consistent, demonstrating the structural integrity 7 (Figure 7d). Wan and co-workers also suggested a combined structural modulation approach to tackle 8 the air-sensitive issue of O3-NaNi_{0.5}Mn_{0.5}O₂. This involves reducing the spacing between Na layers 9 while simultaneously increasing the valence state of Tm, which is achieved by the co-doping of Cu 10 and Ti. Due to the effective suppression of spontaneous phase transition, sodium extraction, and 11 enhanced anti-oxidation capability, the synthesized NaNi_{0.45}Cu_{0.05}Mn_{0.4}Ti_{0.1}O₂ retains its original 12 structure and capacity even after water immersion^[23a](Figure 7e). This improvement results from the 13 suppression of spontaneous sodium extraction and increased antioxidative properties. Zhang and co-14 workers explored beyond the typical O3-type layered Na_xTmO₂ by successfully synthesizing Cu-15 substituted P2-type Na_{0.6}Ni_{0.2}Mn_{0.7}Cu_{0.1}O₂, capitalizing on the high redox potential of Cu²⁺/Cu³⁺ to 16 improve moisture stability by increasing the initial charging potential^[53]. This modification 17 successfully prevented water intercalation. As a result, the optimized P2-Na_{0.6}Ni_{0.2}Mn_{0.7}Cu_{0.1}O₂ 18 maintained its crystal structure even after water treatment and exhibited a high discharge capacity of 19 105.6 mAh g⁻¹ (**Figure 7f**), outperforming that of exposed pristine Na_{0.6}Ni_{0.2}Mn_{0.8}O₂ (60.8 mAh g⁻¹). 20 Other than that, the air-durable $NaFe_{0.4}Mn_{0.49}Cu_{0.1}Zr_{0.01}O_2^{[54]}$, $NaNi_{0.455}Cu_{0.05}Mn_{0.485}Sb_{0.01}O_2^{[56]}$, 21 $Na[Fe_{1/3}Ni_{1/3}Mn_{1/3}]_{0.95}Cu_{0.05}O_{2}^{[57]}$ $NaNi_{1/3}Fe_{1/3}Mn_{1/30.02}Zr_{0.02}O_2^{[58]}$ 22 Na(Ni_{0.4}Cu_{0.1}Mn_{0.4}Ti_{0.1})_{0.999}La_{0.001}O₂^[55] were also demonstrated based on doping or co-doping of Cu, 23 Zr, Sb, or La (**Figure 7g, h**). 24

In addition to transition metal layer doping, sodium layer doping has been identified as another method to enhance the air stability of Na_xTmO₂. Obrovac, Sun, and co-workers reported that compounds such as Na_{0.9}Ca_{0.05}CrO₂ and O3-type Na_{0.98}Ca_{0.01}Ni_{0.5}Mn_{0.5}O₂ significantly delayed spontaneous phase transitions and preserved the original crystal structure^[59]. However, it is important

25

26

27

28

to note that while calcium substitution, as demonstrated in these compounds, can mitigate air sensitivity, it does not entirely eliminate it. More studies are required to further improve air stability.

As discussed, innovations in heteroatom doping and structural modifications, particularly the effective substitution of Tm sites and the incorporation of high-potential redox couples like Cu²⁺/Cu³⁺, have been pivotal in enhancing the air stability of Na_xTmO₂. These advancements play a crucial role in maintaining crystal structures and ensuring the stable electrochemical performance of modified Na_xTmO₂, even in challenging air-exposed environments. This translates into batteries that are not only more durable but also potentially more efficient and reliable. The practical implications of these developments are already visible, as demonstrated by the creation of robust SIBs with significantly improved cathode materials. However, the path forward requires ongoing research. Further refining these approaches has the potential to develop more robust and efficient SIBs, enabling an expanded range of commercial applications.

4.3.3. High-entropy Substitution

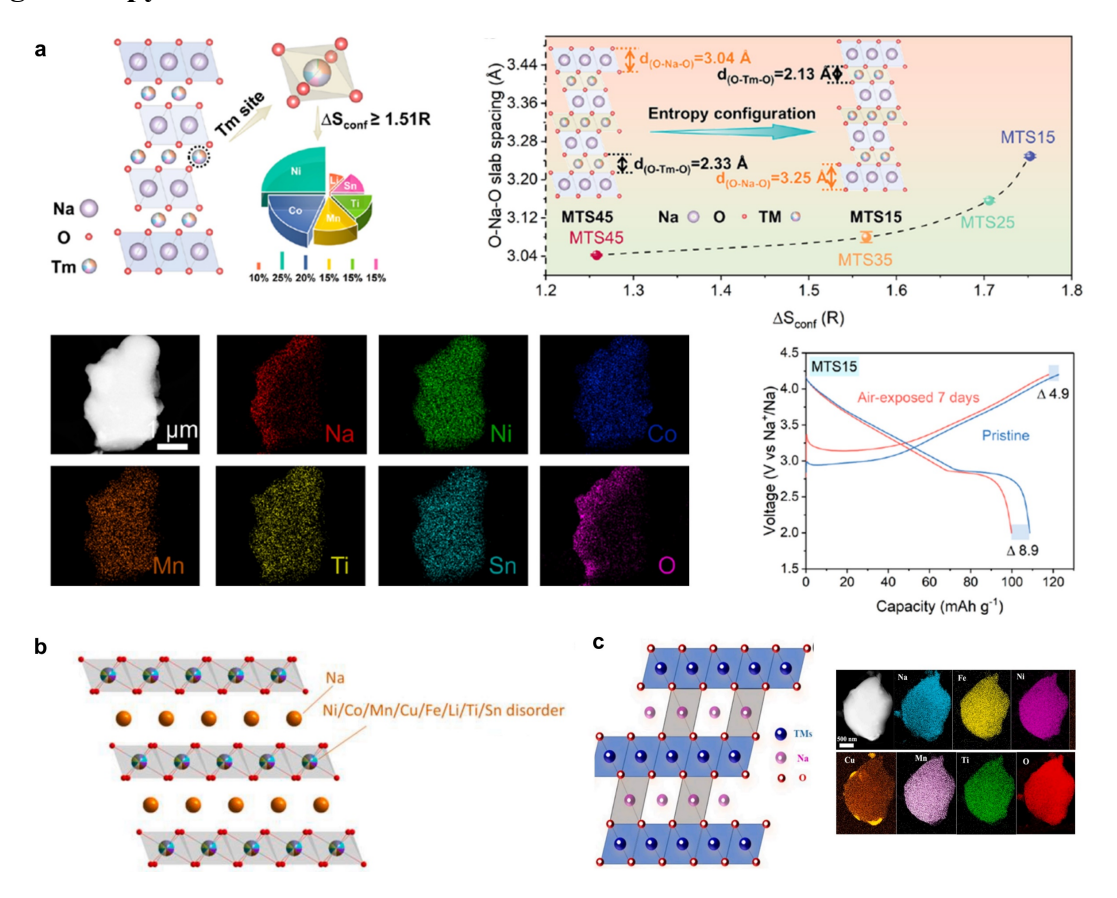


Figure 8. High entropy crystal design for air-compatibility. (a) High entropy crystal structure schematic, configurational entropy, and EDS mapping of Na_{0.83}Li_{0.1}Ni_{0.25}Co_{0.2}Mn_{0.15}Ti_{0.15}Sn_{0.15}O₂ and electrochemical performance of exposed cathode^[60] (Reproduced with permission [REF60], Copyright 2023, ACS Publisher). (b) High entropy crystal structure schematic of NaNi_{0.1}Mn_{0.15}Co_{0.2}Cu_{0.1}Fe_{0.1}Li_{0.1}Ti_{0.15}Sn_{0.1}O₂^[61] (Reproduced with permission [REF61], Copyright 2023, Elsevier Publisher). (c) High entropy crystal structure schematic of NaFe_{0.2}Cu_{0.1}Ni_{0.2}Mn_{0.3}Ti_{0.2}O₂ (left) and EDS mapping (right)^[62] (Reproduced with permission [REF62], Copyright 2023, Elsevier Publisher).

The high-entropy substitution strategy, characterized by the addition of multiple elements in nearly equal proportions into the host structure to increase the entropy and drive structural stabilization, has become a prominent research focus^[63]. Specifically, in the context of high entropy materials, the introduction of various elements influences the Gibbs free energy (ΔG_{mix}) through modifications in both enthalpy (ΔH_{mix}) and entropy (ΔS_{mix}), as described by the equation $\Delta G_{mix} = \Delta H_{mix} - T\Delta S_{mix}$. In certain scenarios, the entropy contribution ($T\Delta S_{mix}$) may offset the enthalpy change (ΔH_{mix}), resulting in a reduction of ΔG_{mix} . This leads to the phenomenon of entropy stabilization, where the negative contribution of $T\Delta S_{mix}$ in the Gibbs–Helmholtz equation effectively outweighs the enthalpy changes associated with mixing, which stabilizes the structure^[61, 64]. The disordered distribution of high-

entropy components tends to promote random redox reactions of metal elements. This characteristic can suppress Na⁺/vacancy ordering, thereby inhibiting phase transition and enhancing structural stability, simultaneously^[62]. In recent years, high-entropy oxides have been proven to have excellent overall performances as cathode materials. For example, Ji and co-workers employed configurational entropy tuning by adjusting the stoichiometric ratios of inactive cations, enabling the precise design of Na-deficient, O3-type Na_xTmO₂ cathodes. Following a 7-day aging period, the high entropy optimized layered Na_{0.83}Li_{0.1}Ni_{0.25}Co_{0.2}Mn_{0.15}Ti_{0.15}Sn_{0.15}O₂ cathodes exhibited a slight decrease in charge and discharge capacities, with a reduction of 4.9 mAh g⁻¹. This minor decrease in capacity underlines the air stability and durability of the entropy-tuned cathode composition^[60] (Figure 8a). Recently, Xiao and co-workers incorporated high-entropy components into the crystal structure of O3-NaNi_{0.5}Mn_{0.5}O₂, significantly improving its tolerance to humidity, even under an ultra-high humid environment (98% relative humidity, 25 °C). The exposed NaNi_{0.1}Mn_{0.15}Co_{0.2}Cu_{0.1}Fe_{0.1}Li_{0.1}Ti_{0.15}Sn_{0.1}O₂ maintained comparative stability in both lattice and electrochemical characteristics after exposure^[61] (**Figure 8b**). In addition, Wang and co-workers developed a layered cathode, NaFe_{0.2}Cu_{0.1}Ni_{0.2}Mn_{0.3}Ti_{0.2}O₂, notable for its air stability. Remarkably, this cathode maintained its morphology and lattice structure even after 7 days of air exposure or 2 to 4 hours of water immersion (Figure 8c). Its air durability is attributed to the entropy stabilization effect and the multicomponent disorder distribution effect^[62].

In short, the high-entropy substitution strategy harnesses the entropic effect, significantly enhancing structural stability and effectively suppressing undesirable phase transitions when exposed to humid environments. The major advantage of this strategy lies in its ability to maintain a disordered distribution of elements, thereby leveraging entropic stabilization. This disorder contributes to the durability and efficiency of SIBs by providing a more robust framework that is less susceptible to degradation under typical operating conditions. These collective findings indicate that high-entropy cathodes represent a promising and forward-thinking direction in the evolution of SIBs, potentially leading to batteries that are not only more efficient but also longer-lasting. However, more mechanism investigation is needed to provide a comprehensive and detailed understanding of the high entropy effect, encompassing from characterization to modeling, to explain the underlying mechanisms more clearly and providing guidance for developing desired Na_xTmO₂.

5. Sustainability and scalability considerations

Along with the aforementioned air stability and electrochemical performance, factors such as environmental impact, cost-effectiveness, and the feasibility of large-scale production are pivotal and significant issues. More effort and attention must be put on exploring sustainability and scalability of SIB techniques, particularly, those using Na_xTmO₂ cathodes enhanced with coatings and dopants entail consideration of the technical challenges of upscaling production while maintaining or enhancing battery performance and durability.

On one hand, in terms of coating strategy, traditional techniques encompass dry^[36,65], wet coatings^[18a,37], and gas-phase chemical coating processes^[35a]. The dry coating method modifies nanoparticles on the cathode mechanically, utilizing surface modification strategies like ball milling or simple mixing. This technique is direct, economical, and can be scaled up easily, making it well-suited for commercial applications that require large-scale production^[65]. In contrast, wet coatings created through sol-gel and solvothermal or hydrothermal techniques are more complex and involve extra costs because of solvent use, which renders them less appropriate for mass production scenarios. Physical Vapor Deposition (PVD), Chemical Vapor Deposition (CVD), and Atomic Layer Deposition (ALD) could provide more precise and consistent thin-film coatings essential for advanced Na_xTmO₂ cathodes. However, their applicability is constrained by high equipment costs, limitations on the materials that can be used, intricate processing requirements, and significant energy demands. Considering these factors, a coating method that enables the formation of homogeneous and stable layers through a cost-effective and scalable dry coating process can be deemed optimal.

On the other hand, when it comes to doping strategy, in the synthesis of Na_xTmO₂, the dopant is systematically introduced into the reaction system in conjunction with the precursors. Subsequently, the integration of the dopant into the lattice structure is facilitated by a process of high-temperature calcination. This methodology effectively ensures the homogeneous distribution of the dopant without introducing supplementary procedural steps into the overarching positive electrode fabrication process. As a result, this approach circumvents the accrual of additional expenditures typically associated with more complex fabrication techniques. Nonetheless, the success of this dopant incorporation strategy hinges critically on the meticulous and judicious design of the dopant element.

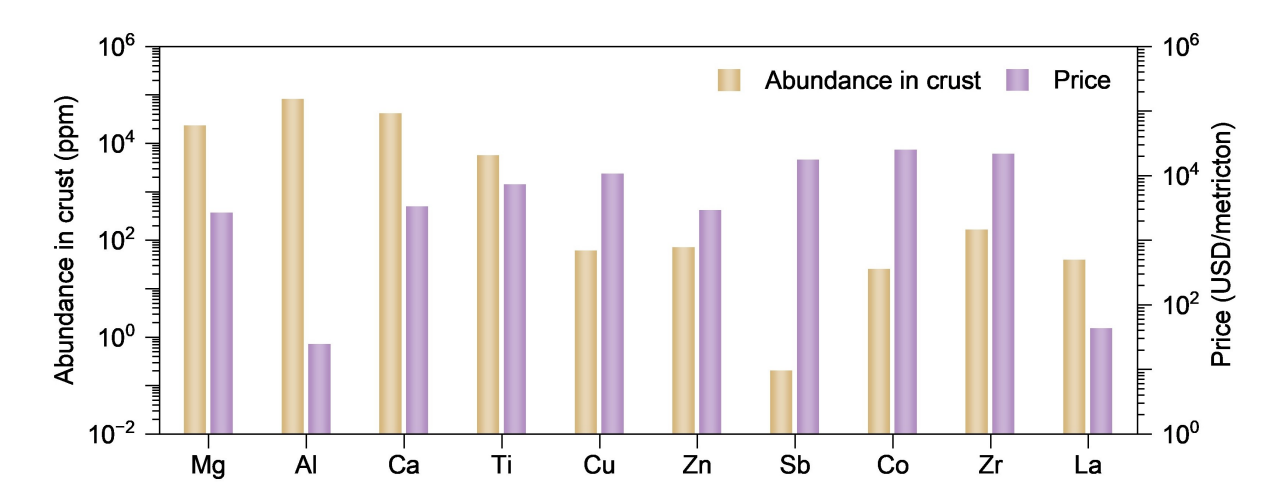


Figure 9. Abundance in crust^[13] and unit price analysis^[14] of coatings and dopants containing Mg, Al, Ca, Ti, Cu, Zn, Sb, Co, Zr, and La (the price is based on their metals).

Beyond the mere technical aspects, the abundance and cost of resources also play crucial roles in evaluating sustainability and scalability. Thus, balancing these factors is essential for the development of Na_xTmO₂. Among the modified Na_xTmO₂ cathodes considered, coatings and dopants based on Mg, Al, Ca, Ti, Cu, Zn, Sb, Co, Zr, and La, each presents unique advantages and challenges. For instance, while dopants like Ti, Co, and rare La offer promising electrochemical and air stability enhancement but raise concerns over cost, availability, and environmental sustainability. Conversely, more abundant, and environmentally benign metal elements such as Mg, Ca, Cu, Zn, and Al present themselves as appealing candidates due to their lower toxicity and acceptable cost (**Figure 9**). Developing effective yet economically and environmentally sustainable dopants and coatings is regarded as the ideal path forward. This involves leveraging the unique features of these elements in terms of high abundance, low cost, and lattice compatibility, while minimizing adverse impacts on battery performance, manufacturing complexity, and the environment. Future studies should explore the combined effects of different dopants, focusing on high-entropy co-substitution and the design of lattice structures. This approach aims to discover dopant combinations that potentially lead to the discovery of innovative Na_xTmO₂ and offer a holistic solution to the challenges of air stability in SIBs.

6. Summary and outlook

The inherent air instability of Na_xTmO_2 presents a significant obstacle in the development of durable cathodes for sustainable and scalable SIBs. This review comprehensively examines the air-induced degradation chemistries of Na_xTmO_2 and the corresponding protective strategies, aiming to elucidate

these complex phenomena and provide new insights for developing air-durable Na_xTmO₂. Degradation is induced by complex interplays among H₂O, CO₂, and the hygroscopic characteristics of Na_xTmO₂, extending from the surface to the bulk phase. Such interactions culminate in the diminution of active Na⁺ and engender the precipitation of hygroscopic sodium compounds, including NaOH, Na₂CO₃, and NaHCO₃, which further accelerate the degradation process. These chemical transformations significantly impair the ion conduction processes and adversely impact the overall performances of SIBs. Simultaneously, these issues pose considerable challenges in cathode manufacturing and battery assembly, not merely constraining the energy output but also amplifying handling costs and the complexity of the fabrication process. This complexity arises from the need for stringent control measures throughout battery design and fabrication to alleviate these effects. Therefore, confronting these challenges and developing an in-depth understanding is pivotal for the advancement of SIBs technology (Figure 10).

Furthermore, this review scrutinizes advanced methodologies designed to enhance the air stability of Na_xTmO₂ in SIBs, providing practical insights for addressing a critical hurdle in their advancement. It evaluates a spectrum of promising techniques, including the deployment of protective coatings, alterations in surface chemistry, structural reconstructions, and the refinement of crystal structures through heteroatom substitution. Among these, the fabrication of a protective layer atop the surface has proven to be a potent tactic, serving as a physical barricade against H₂O and CO₂. Nonetheless, the introduction of coatings that serve as inert components may diminish the overall output energy and power density. An alternative effective strategy encompasses the modification of surface chemistry, notably via washing treatments aimed at excising residual sodium compounds, although the effectiveness is somewhat limited. It is crucial to acknowledge that while such strategies boost air stability, they do not provide an ultimate solution for air-induced degradation. The discourse further highlights the significance of optimizing bulk crystal structure and reengineering surface structure to augment air stability, particularly through controllable heteroatom substitution. This strategy, predicated on altering the inherent atomic and electronic configurations, has been recognized for its profound influence on bolstering intrinsic air stability. The phenomenon is attributed to various mechanisms, such as the spontaneous generation of inert surface oxides, superlattice ordering, modulation of interlayer interactions, or the effect of multicomponent disorder distribution.

Remarkable strides have been made in rendering Na_xTmO₂ air-stable within SIBs, propelled by 1 innovative methodologies like coating applications, surface and structural reconstructions, and 2 heteroatom substitutions.

3

4

5

6

7

8

9

10

11

12

13

14

15

16

17

18

19

20

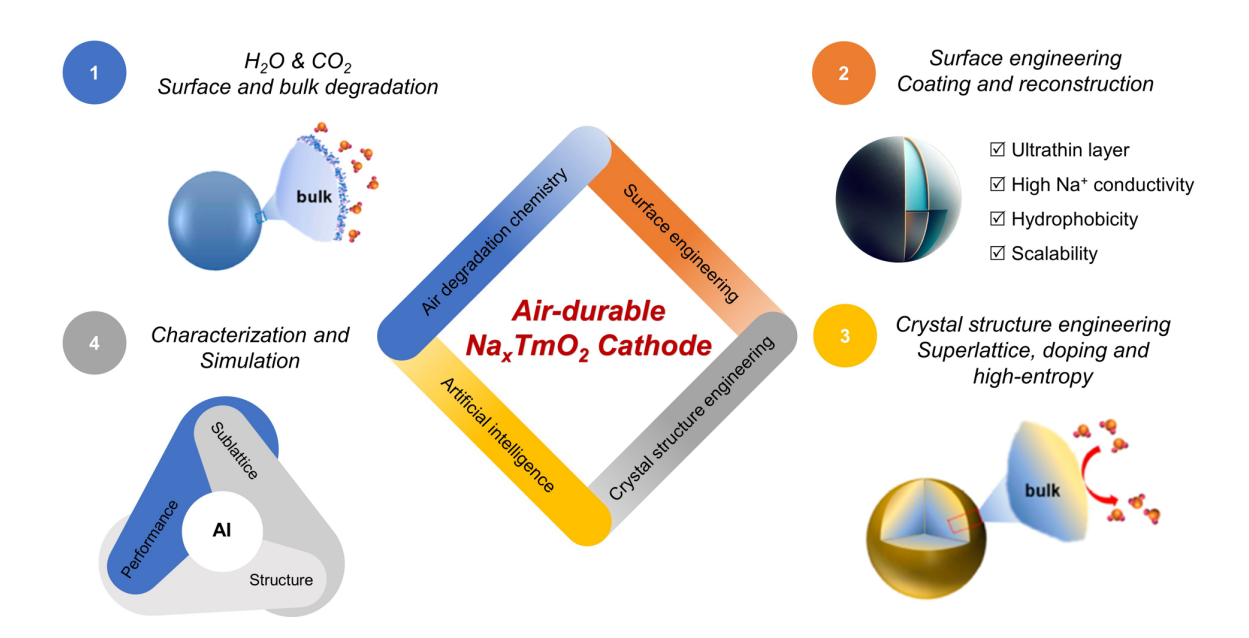


Figure 10. Summary of understanding of degradation and strategy for developing air-stable layered Na_xTmO₂^[18c] (Reproduced with permission [REF18c], Copyright 2022, ACS Publisher).

Amid these advances, unresolved challenges persist, necessitating further scrutiny and research. Future inquiries should focus on refining these strategies, ensuring harmony between effectiveness and practicality, particularly regarding sustainability and scalability. The proven utility of protective coatings calls for the identification of materials that preserve battery capacity and conductivity. Herein, nanotechnology may offer pivotal innovations, facilitating the creation of ultra-thin yet highly efficacious barriers. Beyond mere physical defenses, chemical modifications at the molecular level present a compelling prospect, underscoring the imperative to elucidate the intricate relationship between sublattice structure and performance. This objective might be achieved through sophisticated characterization methodologies and computational simulations, emphasizing the critical role of structural and heteroatom optimization. For instance, high-throughput screening, leveraging a material gene database, facilitates the exclusion of scarce elements in favor of abundant, non-toxic, and costeffective alternatives, especially prioritizing those that promise sustainability and accessibility without compromising on quality or functionality. Furthermore, leveraging advanced computational models and machine learning algorithms could dramatically transform the prediction and design of crystal

structures inherently resistant to air-induced degradation, potentially reducing the trial-and-error 1 approach prevalent in materials development and accelerating the discovery of novel, more effective 2 cathodes. However, each proposed strategy introduces its own challenges, including the cost and 3 complexity of synthesizing advanced materials. Identifying chemical treatments that enhance stability 4 without yielding negative repercussions remains crucial, possibly through innovative compounds or 5 more efficient synthesis and processing techniques. Moreover, the practical implementation of these 6 strategies demands comprehensive testing across varied conditions to assess long-term stability, 7 performance at extreme temperatures, and scalability for industrial production, necessitating thorough 8 examination. 9

In conclusion, significant progress has been achieved in improving the air stability of SIB cathodes. However, the development toward optimizing these cathodes is far from complete. Continuous research is essential to overcome the existing challenges. The overarching goal is to develop batteries that not only exhibit superior air stability but also meet the criteria of energy efficiency, environmental sustainability, and economic viability. This endeavor is critical in the evolving field of sustainable and scalable energy storage technologies, where the balance between performance and practicality is paramount.

Credit author statement

10

11

12

13

14

15

16

17

21

24

- Zheng Chen: Supervision, Funding acquisition, Conceptualization, Writing-Reviewing and Editing.
- 19 Feng Li, Wei Tang, Junlin Wu, Lanshuang Zhang, and Anthony Mu: Conceptualization, Writing-
- Original Draft, Figures Organize, Reviewing, Editing, and Proof Reading.

Declaration of competing interest

- The authors declare that they have no known competing financial interests or personal relationships
- that could have appeared to influence the work reported in this paper.

Data availability

This is a review paper.

1 Acknowledgment

- 2 Funding to support this work was provided by the National Science Foundation through the Future
- 3 Manufacturing (FM) grant no. 2134764.

4 References

- 5 [1] F. Wang, J. D. Harindintwali, Z. Yuan, M. Wang, F. Wang, S. Li, Z. Yin, L. Huang, Y. Fu, L. Li,
- 6 Innovation. **2021**, 2, 100180.
- [2] a) C. Vaalma, D. Buchholz, M. Weil, S. Passerini, Nat. Rev. Mater. 2018, 3, 1; b) F. Duffner, N.
- 8 Kronemeyer, J. Tübke, J. Leker, M. Winter, R. Schmuch, Nat. Energy 2021, 6, 123; c) D. Larcher, J.-
- 9 M. Tarascon, Nat. Chem. 2015, 7, 19; d) N. Yabuuchi, K. Kubota, M. Dahbi, S. Komaba, Chem. Rev.
- 2014, 114, 11636; e) J.-Y. Hwang, S.-T. Myung, Y.-K. Sun, Chem. Soc. Rev. 2017, 46, 3529; f) R.
- Usiskin, Y. Lu, J. Popovic, M. Law, P. Balaya, Y.-S. Hu, J. Maier, Nat. Rev. Mater. 2021, 6, 1020.
- 12 [3] a) J. Deng, W. B. Luo, S. L. Chou, H. K. Liu, S. X. Dou, Adv. Energy Mater. 2018, 8, 1701428; b)
- M. Li, Z. Du, M. A. Khaleel, I. Belharouak, Energy Stor. Mater. 2020, 25, 520; c) Y. Huang, Y. Zheng,
- 14 X. Li, F. Adams, W. Luo, Y. Huang, L. Hu, ACS Energy Lett. 2018, 3, 1604; d) Y. Li, Y. Lu, C. Zhao,
- 15 Y.-S. Hu, M.-M. Titirici, H. Li, X. Huang, L. Chen, *Energy Stor. Mater.* **2017**, 7, 130; e) Y. Tian, G.
- Zeng, A. Rutt, T. Shi, H. Kim, J. Wang, J. Koettgen, Y. Sun, B. Ouyang, T. Chen, *Chem. Rev.* 2020,
- 17 121, 1623.
- [4] P. W. Gruber, P. A. Medina, G. A. Keoleian, S. E. Kesler, M. P. Everson, T. J. Wallington, J. Ind.
- 19 *Ecol.* **2011**, 15, 760.
- ²⁰ [5] M. Zhang, Y. Li, F. Wu, Y. Bai, C. Wu, *Nano Energy* **2021**, 82, 105738.
- [6] K. Chayambuka, G. Mulder, D. L. Danilov, P. H. Notten, *Adv. Energy Mater.* **2020**, 10, 2001310.
- [7] C. Zhao, Q. Wang, Z. Yao, J. Wang, B. Sánchez-Lengeling, F. Ding, X. Qi, Y. Lu, X. Bai, B. Li,
- 23 Science **2020**, 370, 708.
- 24 [8] a) Q. Liu, Z. Hu, M. Chen, C. Zou, H. Jin, S. Wang, S. L. Chou, S. X. Dou, Small 2019, 15,
- 25 1805381; b) J.-M. Kim, X. Zhang, J.-G. Zhang, A. Manthiram, Y. S. Meng, W. Xu, *Mater. Today* **2021**,
- ²⁶ 46, 155; c) M. H. Han, E. Gonzalo, G. Singh, T. Rojo, *Energy Environ. Sci.* **2015**, 8, 81.
- 27 [9] a) J. Peng, W. Zhang, Q. Liu, J. Wang, S. Chou, H. Liu, S. Dou, *Adv. Mater.* **2022**, 34, 2108384;
- 28 b) K. Hurlbutt, S. Wheeler, I. Capone, M. Pasta, *Joule* **2018**, 2, 1950; c) W. J. Li, C. Han, G. Cheng,

- S. L. Chou, H. K. Liu, S. X. Dou, Small 2019, 15, 1900470.
- [10]a) P. Barpanda, L. Lander, S. i. Nishimura, A. Yamada, *Adv. Energy Mater.* **2018**, 8, 1703055; b)
- Q. Ni, Y. Bai, F. Wu, C. Wu, Adv. Sci. 2017, 4, 1600275; c) L. Zhao, T. Zhang, H. Zhao, Y. Hou, Mater.
- 4 *Today Nano* **2020**, 10, 100072.
- ⁵ [11]a) K. Kubota, N. Yabuuchi, H. Yoshida, M. Dahbi, S. Komaba, *Mrs Bull.* **2014**, 39, 416; b) J. Y.
- 6 Hwang, J. Kim, T. Y. Yu, Y. K. Sun, *Adv. Energy Mater.* **2019**, 9, 1803346; c) Y. Liu, Y.-H. Zhang, J.
- ⁷ Ma, J. Zhao, X. Li, G. Cui, *Chem. Mater.* **2023**.
- 8 [12]H. Battery, *Na-Ion Battery*, <u>https://www.hinabattery.com/en/index.php?catid=12</u> **2017**.
- 9 [13] Abundance of chemical elements in Earth's (continental) crust,
- 10 https://en.wikipedia.org/wiki/Abundance of elements in Earth%27s crust 2024.
- [14] SMM Spot Metal Prices, https://www.metal.com/ 2024.
- 12 [15] A. Bauer, J. Song, S. Vail, W. Pan, J. Barker, Y. Lu, Adv. Energy Mater. 2018, 8, 1702869.
- [16] V. Palomares, P. Serras, I. Villaluenga, K. B. Hueso, J. Carretero-González, T. Rojo, Energy
- 14 Environ. Sci. 2012, 5, 5884.
- 15 [17]a) H.-R. Yao, L. Zheng, S. Xin, Y.-G. Guo, Sci. China Chem. 2022, 65, 1076; b) H. S. Hirsh, Y. Li,
- D. H. Tan, M. Zhang, E. Zhao, Y. S. Meng, *Adv. Energy Mater.* **2020**, 10, 2001274.
- 17 [18]a) Y. You, A. Dolocan, W. Li, A. Manthiram, *Nano Lett.* **2018**, 19, 182; b) Z. Lu, J. Dahn, *Chem.*
- Mater. 2001, 13, 1252; c) W. Zuo, Z. Xiao, M. Zarrabeitia, X. Xue, Y. Yang, S. Passerini, ACS Mater.
- 19 Lett. 2022, 4, 1074; d) R. Zhang, S. Yang, H. Li, T. Zhai, H. Li, InfoMat 2022, 4, e12305.
- ²⁰ [19]a) J. Wang, Y.-F. Zhu, Y. Su, J.-X. Guo, S. Chen, H.-K. Liu, S.-X. Dou, S.-L. Chou, Y. Xiao, *Chem.*
- Soc. Rev. 2024; b) S. Jia, S. Kumakura, E. McCalla, Energy Environ. Sci. 2024.
- 22 [20] C. Delmas, C. Fouassier, P. Hagenmuller, *Phys. B+C* **1980**, 99, 81.
- 23 [21]a) T. Liu, J. Liu, L. Li, L. Yu, J. Diao, T. Zhou, S. Li, A. Dai, W. Zhao, S. Xu, Nature 2022, 606,
- 305; b) W. Lin, W. Bao, J. Cai, X. Cai, H. Zhao, Y. Zhang, Y. Deng, S. Yang, Z. Zhou, Z. Liu, Appl.
- 25 Surf. Sci. 2023, 615, 156278.
- ²⁶ [22] W. Zuo, J. Qiu, X. Liu, F. Ren, H. Liu, H. He, C. Luo, J. Li, G. F. Ortiz, H. Duan, J. Liu, M.-S.
- 27 Wang, Y. Li, R. Fu, Y. Yang, Nat. Commun. 2020, 11, 3544.
- 28 [23]a) H.-R. Yao, P.-F. Wang, Y. Gong, J. Zhang, X. Yu, L. Gu, C. OuYang, Y.-X. Yin, E. Hu, X.-Q.
- 29 Yang, J. Am. Chem. Soc. 2017, 139, 8440; b) K. Kubota, S. Komaba, J Electrochem. Soc. 2015, 162,
- A2538; c) M. Sathiya, K. Hemalatha, K. Ramesha, J.-M. Tarascon, A. Prakash, *Chem. Mater.* 2012,

- 1 24, 1846.
- [24] S. Lee, S. W. Doo, M. S. Jung, S. G. Lim, K. Kim, K. T. Lee, *J. Mater. Chem. A* **2021**, 9, 14074.
- [25]a) M. Han, N. Sharma, E. Gonzalo, J. Pramudita, H. Brand, J. L. Del Amo, T. Rojo, J. Mater.
- 4 Chem. A 2016, 4, 18963; b) L. Mu, S. Xu, Y. Li, Y. S. Hu, H. Li, L. Chen, X. Huang, Adv. Mater. 2015,
- 5 27, 6928.
- 6 [26] Y. You, B. Song, K. Jarvis, A. Huq, A. Manthiram, *ACS Mater. Lett.* **2019**, 1, 89.
- ⁷ [27] S. Roberts, L. Chen, B. Kishore, C. E. Dancer, M. J. Simmons, E. Kendrick, *J. Colloid Interf. Sci.*
- 8 **2022**, 627, 427.
- 9 [28] X. Li, X. Shen, J. Zhao, Y. Yang, Q. Zhang, F. Ding, M. Han, C. Xu, C. Yang, H. Liu, ACS Appl.
- 10 *Mater. Interfaces* **2021**, 13, 33015.
- [29] C. Shi, L. Wang, X. a. Chen, J. Li, S. Wang, J. Wang, H. Jin, *Nanoscale Horizons* **2022**, 7, 338.
- 12 [30] W. M. Seong, Y. Kim, A. Manthiram, *Chem. Mater.* **2020**, 32, 9479.
- [31]a) S. Lux, I. Lucas, E. Pollak, S. Passerini, M. Winter, R. Kostecki, *Electrochem. Commun.* 2012,
- 14, 47; b) P. Barnes, K. Smith, R. Parrish, C. Jones, P. Skinner, E. Storch, Q. White, C. Deng, D.
- 15 Karsann, M. L. Lau, *J. Power Sources* **2020**, 447, 227363.
- [32] P. Guan, L. Zhou, Z. Yu, Y. Sun, Y. Liu, F. Wu, Y. Jiang, D. Chu, *Journal of Energy Chemistry*
- **2020**, 43, 220.
- 18 [33] J. Li, H. Hu, J. Wang, Y. Xiao, Carbon Neutralization 2022, 1, 96.
- 19 [34] C.-Y. Yu, J.-S. Park, H.-G. Jung, K.-Y. Chung, D. Aurbach, Y.-K. Sun, S.-T. Myung, Energy
- 20 Environ. Sci. 2015, 8, 2019.
- [35]a) L. Yang, S. Sun, K. Du, H. Zhao, D. Yan, H. Y. Yang, C. Yu, Y. Bai, Ceram. Int. **2021**, 47, 28521;
- b) Y. Liu, X. Fang, A. Zhang, C. Shen, Q. Liu, H. A. Enaya, C. Zhou, *Nano Energy* **2016**, 27, 27.
- 23 [36] J. Lamb, A. Manthiram, ACS Appl. Energy Mater. **2021**, 4, 11735.
- [37] D. Park, M. Choi, M. Kim, J.-H. Park, H.-S. Kim, W. Choi, *Appl. Energy* **2023**, 349, 121639.
- 25 [38]a) A. M. Wise, C. Ban, J. N. Weker, S. Misra, A. S. Cavanagh, Z. Wu, Z. Li, M. S. Whittingham,
- 26 K. Xu, S. M. George, *Chem. Mater.* **2015**, 27, 6146; b) W. Zhu, X. Huang, T. Liu, Z. Xie, Y. Wang, K.
- 27 Tian, L. Bu, H. Wang, L. Gao, J. Zhao, *Coatings* **2019**, 9, 92.
- [39] Y. Wang, K. Tang, X. Li, R. Yu, X. Zhang, Y. Huang, G. Chen, S. Jamil, S. Cao, X. Xie, *Chem.*
- 29 Eng. J. **2019**, 372, 1066.
- [40] L. Zheng, L. Li, R. Shunmugasundaram, M. Obrovac, ACS Appl. Mater. Interfaces 2018, 10,

- 1 38246.
- ² [41] S. Guo, Q. Li, P. Liu, M. Chen, H. Zhou, *Nat. Commun.* **2017**, 8, 135.
- ³ [42] J. Y. Li, H. Y. Hu, L. F. Zhou, H. W. Li, Y. J. Lei, W. H. Lai, Y. M. Fan, Y. F. Zhu, G. Peleckis, S.
- 4 Q. Chen, Adv. Funct. Mater. 2023, 33, 2213215.
- 5 [43]a) R. Moshtev, P. Zlatilova, S. Vasilev, I. Bakalova, A. Kozawa, J. Power Sources 1999, 81, 434;
- 6 b) X. Zheng, X. Li, Z. Wang, H. Guo, Z. Huang, G. Yan, D. Wang, *Electrochim. Acta* **2016**, 191, 832.
- ⁷ [44] K. Jiang, S. Xu, S. Guo, X. Zhang, X. Zhang, Y. Qiao, T. Fang, P. Wang, P. He, H. Zhou, Nano
- 8 Energy **2018**, 52, 88.
- 9 [45]a) H.-R. Yao, W.-J. Lv, Y.-X. Yin, H. Ye, X.-W. Wu, Y. Wang, Y. Gong, Q. Li, X. Yu, L. Gu, ACS
- Appl. Mater. Interfaces 2019, 11, 22067; b) J. Vinckeviciute, M. D. Radin, A. Van der Ven, Chem.
- 11 *Mater.* **2016**, 28, 8640.
- 12 [46]a) Y. Qi, Q. Xu, A. Van der Ven, J Electrochem. Soc. 2012, 159, A1838; b) W. H. Woodford, Y.-
- 13 M. Chiang, W. C. Carter, *J Electrochem. Soc.* **2013**, 160, A1286; c) A. J. Toumar, S. P. Ong, W. D.
- 14 Richards, S. Dacek, G. Ceder, *Phys. Rev. Appl.* **2015**, 4, 064002.
- 15 [47] P. F. Wang, M. Weng, Y. Xiao, Z. Hu, Q. Li, M. Li, Y. D. Wang, X. Chen, X. Yang, Y. Wen, Adv.
- 16 *Mater.* **2019**, 31, 1903483.
- 17 [48] L. Gan, X. G. Yuan, J. J. Han, X. Yang, L. Zheng, Z. Huang, H. R. Yao, Adv. Funct. Mater. 2023,
- 18 33, 2209026.
- 19 [49] L. Gan, X. G. Yuan, J. J. Han, J. Li, L. Zheng, H. R. Yao, Carbon Neutralization 2023, 2, 235.
- ²⁰ [50] P.-F. Wang, H.-R. Yao, X.-Y. Liu, Y.-X. Yin, J.-N. Zhang, Y. Wen, X. Yu, L. Gu, Y.-G. Guo, *Sci.*
- 21 Adv. **2018**, 4, eaar6018.
- [51] X. Meng, D. Zhang, Z. Zhao, Y. Li, S. Xu, L. Chen, X. Wang, S. Liu, Y. Wu, J. Alloys Compd.
- **2021**, 887, 161366.
- ²⁴ [52] Y. Xiao, T. Wang, Y.-F. Zhu, H.-Y. Hu, S.-J. Tan, S. Li, P.-F. Wang, W. Zhang, Y.-B. Niu, E.-H.
- 25 Wang, *Research* **2020**.
- [53] J. Jiang, H.-C. He, C. Cheng, T. Yan, X. Xia, M. Ding, L. He, T.-S. Chan, L. Zhang, ACS Appl.
- 27 Energy Mater. **2022**, 5, 1252.
- [54] Y.-M. Zheng, X.-B. Huang, X.-M. Meng, S.-D. Xu, L. Chen, S.-B. Liu, D. Zhang, ACS Appl.
- 29 *Mater. Interfaces* **2021**, 13, 45528.
- ³⁰ [55] Q. Zhang, Z. Wang, X. Li, H. Guo, W. Peng, J. Wang, G. Yan, *Chem. Eng. J.* **2022**, 431, 133456.

- [56] Y. Jin, Y. Li, J. Li, H. Zhou, X. Chen, P. Jiang, Q. Fan, Q. Kuang, Y. Dong, Y. Zhao, ACS Appl.
- 2 *Energy Mater.* **2024**.
- ³ [57] X. Xu, G. Liu, C. Su, Y. Zhang, L. Wen, *Ionics* **2024**, 1.
- [58] C. Jiang, Y. Wang, Y. Xin, X. Ding, S. Liu, Y. Pang, B. Chen, Y. Wang, L. Liu, F. Wu, Carbon
- 5 Neutralization **2024**.
- 6 [59]a) T.-Y. Yu, J. Kim, J.-Y. Hwang, H. Kim, G. Han, H.-G. Jung, Y.-K. Sun, J. Mater. Chem. A 2020,
- ⁷ 8, 13776; b) L. Zheng, J. C. Bennett, M. Obrovac, *J Electrochem. Soc.* **2019**, 166, A2058.
- 8 [60] H. Wang, X. Gao, S. Zhang, Y. Mei, L. Ni, J. Gao, H. Liu, N. Hong, B. Zhang, F. Zhu, ACS Nano
- 9 **2023**, 17, 12530.
- [61] X.-Y. Du, Y. Meng, H. Yuan, D. Xiao, Energy Stor. Mater. 2023, 56, 132.
- [62] Y. Dang, Z. Xu, H. Yang, K. Tian, Z. Wang, R. Zheng, H. Sun, Y. Liu, D. Wang, Appl. Surf. Sci.
- **2023**, 636, 157856.
- [63] Y. Chen, H. Fu, Y. Huang, L. Huang, X. Zheng, Y. Dai, Y. Huang, W. Luo, ACS Mater. Lett. 2020,
- 14 3, 160.
- 15 [64]a) S. Schweidler, M. Botros, F. Strauss, Q. Wang, Y. Ma, L. Velasco, G. Cadilha Marques, A.
- Sarkar, C. Kübel, H. Hahn, Nat. Rev. Mater. 2024, 1; b) Y. Ma, Y. Ma, Q. Wang, S. Schweidler, M.
- Botros, T. Fu, H. Hahn, T. Brezesinski, B. Breitung, Energy Environ. Sci. 2021, 14, 2883; c) H. Gao,
- J. Li, F. Zhang, C. Li, J. Xiao, X. Nie, G. Zhang, Y. Xiao, D. Zhang, X. Guo, Adv. Energy Mater. 2024,
- 19 2304529.

21

²⁰ [65] Y. Lee, C. Park, K. Park, *Chem. Mater.* **2023**, 36, 232.